GEOLOGY

Heavy potassium isotopes in carbonatites reveal oceanic crust subduction as the driver of deep carbon cycling

Zheng-Yu Long[1,2]*, Frédéric Moynier[1]*, Baptiste Debret[1], Kun-Feng Qiu[2]*, Wei Dai[1], Hao-Xuan Sun[1], Jun Deng[2], Hervé Bertrand[3], Kevin Burton[4], Edward Inglis[5], Sebastian Tappe[6,7]

Carbon cycling between surface and mantle reservoirs is pivotal in fostering habitability of Earth. A critical yet poorly constrained parameter is whether crustal carbon can "survive" devolatilization processes that accompany slab subduction and therefore influence deep carbon budgets. Carbonatites provide a key record to address this important topic. Here, we present high-precision potassium isotope data for a large set of carbonatite samples from both continental and oceanic settings, spanning from 2 billion years ago to the present. Modeling suggests that the heavy potassium isotopic compositions of carbonatites are inherited from their mantle sources, rather than resulting from magmatic and postmagmatic processes. Our results demonstrate a strong link between the subduction of oceanic crust and the recycling of carbonates into the mantle sources of carbonatites. These findings support the hypothesis that subduction of carbonate-bearing altered oceanic crust has been a critical mechanism for transferring carbon into the deep Earth through time.

INTRODUCTION

The geological cycles and interactions of volatile elements, particularly those involving carbon, influence the long-term evolution of climate, ocean, and life (*1*–*4*). The carbon cycle is characterized by the ongoing release of carbon from the mantle via volcanism and reintroduction into the mantle via plate subduction (*5*, *6*). Subducted materials such as limestone- and chalk-bearing calcareous sedimentary successions (*7*), ophicarbonates (*8*, *9*), and altered basaltic oceanic crust (*10*, *11*) are primary carbon carriers into subduction zones. However, metamorphic dehydration and melting during subduction may return subducted carbon back to the surface via arc magmatism or sedimentary accretion to active continental margins (*12*–*14*), thereby limiting the extent of deep carbon cycle. This has sparked a vigorous debate about whether carbon contained in downgoing slabs can be effectively recycled into the deep Earth.

Magmatism is essential to Earth's carbon cycle, bridging the mantle and surface through a complex interaction of crustal recycling, mantle storage, and volcanism (*2*, *3*). Important advances in understanding the relationship between surface carbon and mantle reservoirs are based on the investigation of samples from oceanic hotspots, e.g., ocean island basalts (OIBs). Previous studies revealed that certain OIBs carry geochemical imprints of marine carbonates, suggesting the preservation of crustal carbon in the deep mantle (*15*–*18*). However, the limited preservation of oceanic hotspots to approximately the last 200 million years (Ma) challenges our understanding of the deep carbon cycle through geological time. Moreover, the geochemical signature of recycled carbonates might be diluted in OIBs due to the high-degree partial melting of the peridotite-dominated mantle.

Carbonatites are derived from low-degree melts of volatile-rich mantle sources (*19*–*21*). These rare magmatic rocks are predominantly found in cratonic areas and continental rifts, and some occur within or in the vicinity of orogenic belts and oceanic plateaus (*19*). The $^{143}Nd/^{144}Nd$ and $^{176}Hf/^{177}Hf$ ratios of global carbonatites align with the respective isotope evolutionary path of the chondritic or primitive mantle (fig. S1), suggesting an ultimate origin from the convecting upper mantle. Plume-lithosphere interaction has also been advocated for the generation of some carbonatites (*20*–*22*). Evidence from boron isotopes reveals the recycling of crustal materials into the mantle sources of global carbonatite magmatism (*23*). Although the crustal signatures are either sampled from the ambient convecting mantle or from metasomatized lithospheric mantle after plume impact (*22*, *24*–*26*), they ultimately originated from subducted slabs introduced into the deeper mantle. Despite diverse components in the mantle sources of carbonatites (*26*–*29*), these rocks crystallize from oxidized magmas (*30*), which require the addition of oxidized metasomatic agents such as subducted carbonates to the mantle sources (*31*).

The critical role of recycled marine carbonates in the petrogenesis of some carbonatites has been evidenced by their calcium (*28*, *32*) and magnesium (*33*, *34*) isotopic signatures. However, the effectiveness of these tracers remains incompletely understood. For instance, a global study of carbonatites proposed that recycled carbonates do not substantially influence the calcium isotopic signatures of carbonatites (*35*). Instead, magnesium and calcium, as major elements of mantle minerals, can undergo isotopic fractionation during peridotite partial melting, particularly when phases such as spinel and garnet are present (*36*, *37*). Moreover, the formation of carbonatites typically involves liquid immiscibility following the differentiation of parental CO_2-bearing silicate melts, wherein the lighter isotopes of calcium and magnesium are preferentially incorporated into the

[1]Université Paris Cité, Institut de Physique du Globe de Paris, CNRS, 75005 Paris, France. [2]Frontiers Science Center for Deep-time Digital Earth, State Key Laboratory of Geological Processes and Mineral Resources, School of Earth Sciences and Resources, China University of Geosciences, Beijing, China. [3]Laboratoire de Geologie de Lyon, Ecole normale supérieure de Lyon, Lyon, France. [4]Department of Earth Sciences, Durham University, Elvet Hill, Durham DH1 3LE, UK. [5]School of Earth and Environmental Science, Main Building, Cardiff University, Cardiff, Wales CF10 3AT, UK. [6]Department of Geosciences, UiT The Arctic University of Norway, 9037 Tromsø, Norway. [7]Institute for Mineralogy, Technical University Bergakademie Freiberg, D-09599 Freiberg, Germany.
*Corresponding author. Email: long@ipgp.fr (Z.-Y.L.); moynier@ipgp.fr (F.M.); kunfengqiu@qq.com (K.-F.Q.)

carbonatite melt fraction (*38*, *39*). These isotope fractionation effects are similar to those produced by the addition of carbonates to the Earth's mantle.

Carbonate-rich sediments entering subduction zones are commonly interbedded with clay-rich layers or rest atop altered igneous oceanic crust. Although potassium is not structurally incorporated into carbonate minerals, it concentrates primarily in such clay-rich sediments and altered igneous oceanic crust, which also act as primary carriers for subducting carbon (*6*, *40*). Marine carbonate sediments generally include substantial clay and other silicate fractions containing substantial K_2O (typically 1 to 5 wt %), while altered oceanic crust (AOC) acquires K-bearing minerals (e.g., smectite and K-feldspar) through seafloor hydrothermal alteration (*31*, *41*, *42*). Thus, wherever carbon enters subduction zones, potassium accompanies it, either in interbedded clay-rich sediments or within altered basaltic crust underlying the carbonates (*10*, *11*). Because of its strong incompatibility and sensitivity to fluid-related processes, potassium effectively traces dehydration, fluid transfer, and melt recycling from slabs into the mantle—a process frequently associated with the mobilization or buffering of subducted carbon (as CO_2). When such carbonate-bearing oceanic slabs are subducted beyond volcanic arc depths, their geochemical signatures may reappear in deeply derived mantle melts such as carbonatites or OIBs. Thus, potassium isotopes can reflect the mass flux and nature of subducted materials (*43*–*46*).

In this context, potassium isotopes represent a promising proxy for identifying carbonate-rich recycled components in carbonatite magmas. Although a pure carbonate layer may be essentially invisible to potassium isotopes because of its negligible potassium content, associated clay-rich sedimentary or altered basaltic components may impart measurable potassium isotopic signals. Furthermore, potassium isotopes provide unique advantages as geochemical tracers: (i) Potassium is highly incompatible during partial melting of the mantle; thus, mantle melting does not cause any substantial potassium isotopic fractionation (*47*). (ii) Potassium isotopic fractionation is limited during the formation of these magmas because potassium is incompatible in near-liquidus fractionating minerals such as olivine, pyroxene, magnetite, calcite, and apatite (*47*–*49*) (further details in Discussion). (iii) Potassium isotopes have proven sensitive to source variability in mantle-derived magmas (*41*, *43*–*45*, *50*). (iv) The well-defined equilibrium fractionation factor between minerals and melts/fluids provides a robust basis for quantitative assessments of potential potassium isotopic variation during magmatic processes (*51*, *52*).

In this study, we analyzed the potassium isotopic compositions of 38 carbonatites from 14 occurrences worldwide, encompassing continental and oceanic settings, spanning from 2 billion years ago (Ga) to the present (Fig. 1; detailed sample information in tables S1 and S2). We first investigate potassium isotopic fractionation during hydrothermal alteration by comparing samples previously identified as hydrothermally altered with "primary" carbonatites (i.e., those free of hydrothermal alteration and supergene weathering). Then, on the basis of our leaching experiments and previous first-principles calculations, we use quantitative modeling to examine potassium isotopic behavior during magmatic differentiation. We also use potassium isotope data in combination with Monte Carlo simulations to test the hypothesis that the mantle source of carbonatites contains a carbonate component derived from subducting slabs. Last, we explore the implications of our data for carbonatite genesis and their role in the deep carbon cycle.

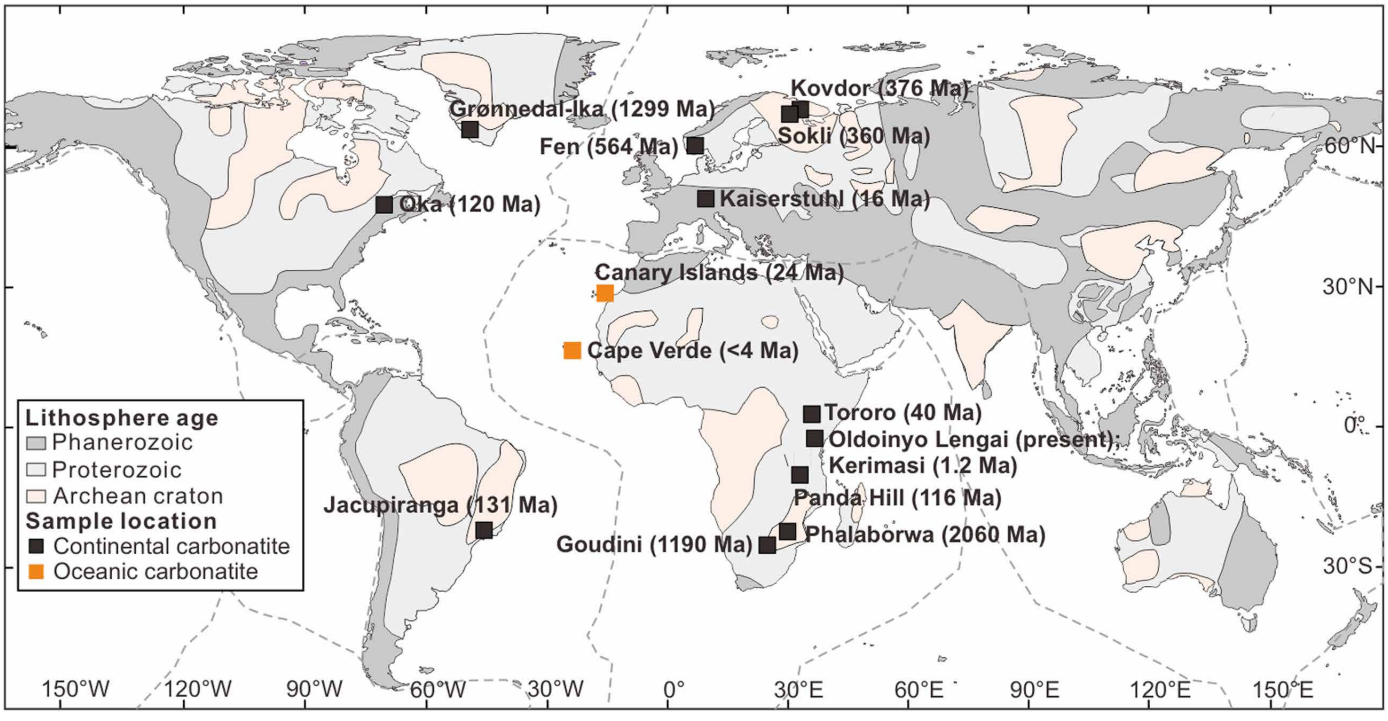

Fig. 1. Locations of the investigated carbonatites from this study. Although carbonatites are mostly found in continental settings, rare samples from two oceanic occurrences (Canary Islands and Cape Verde) were included in this potassium isotope study. More information on samples is detailed in tables S1 and S2.

RESULTS

The results of potassium concentrations and isotopic compositions are listed in table S3. The $\delta^{41}K$ values of most carbonate separates are consistent with the $\delta^{41}K$ values of the corresponding whole-rock analyses within analytical uncertainties (Fig. 2). For more than 80% of the samples, >40% of the total potassium budget is hosted in the carbonate separates (Fig. 2), which indicates that the bulk potassium budget of investigated carbonatites is mainly controlled by carbonate minerals. This reflects that potassium is highly incompatible in most silicate, phosphate, and oxide minerals in carbonatites, such as olivine, apatite, and magnetite, with relatively common K-rich phlogopite being a notable exception. The samples with the lowest proportion of potassium hosted in carbonates (40 and 60% in samples P23 and P24 from Fen and 91/66-C2 from Jacupiranga) suggest the presence of minor phlogopite (tables S1 and S2). Nevertheless, the measured $\delta^{41}K$ difference between bulk and carbonate analyses is very small (Fig. 2).

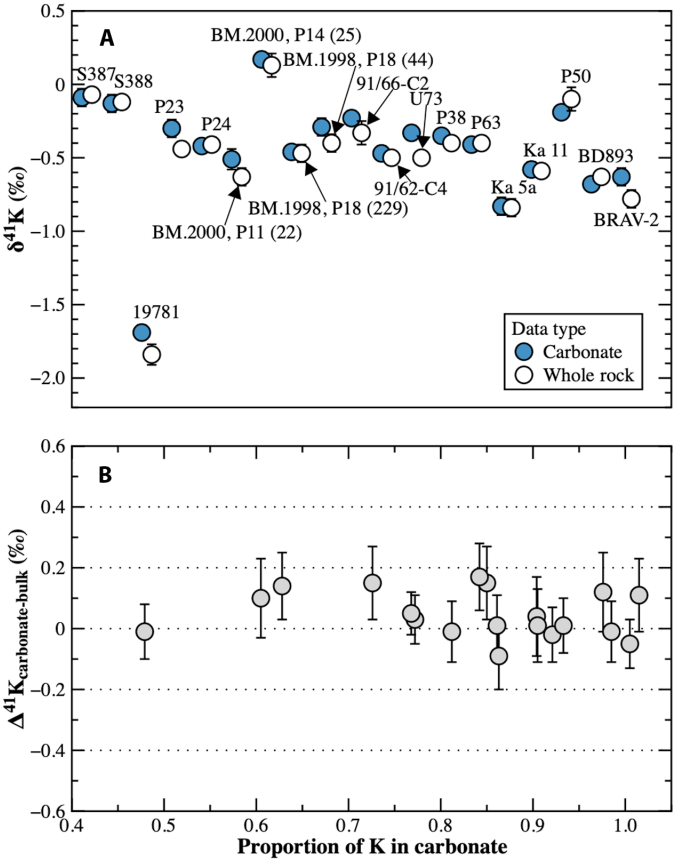

Fig. 2. Comparison of potassium contents and isotopic compositions between carbonate mineral and whole rock for the investigated carbonatites. (**A**) Displays $\delta^{41}K$ values for 19 selected carbonatite samples, comparing carbonate and whole-rock measurements. (**B**) Relationship between the proportion of potassium in carbonate and the potassium isotopic variation ($\Delta^{41}K_{carbonate\text{-}bulk}$). Our results predominantly show $\Delta^{41}K_{carbonate\text{-}bulk}$ = ~0 and no systematic variation with the proportion of potassium, suggesting that silicate and carbonate minerals are isotopically equilibrated in terms of potassium. The data for carbonate minerals are obtained from the carbonate-dissolved solution, while the whole-rock data represent measurements from bulk rock analysis. For information on the creation of the two groups, refer to Materials and Methods.

The Paleo- and Mesoproterozoic samples from Phalaborwa [−0.12 ± 0.04 to −0.07 ± 0.03 per mil (‰)] and Goudini (−0.05 ± 0.07‰) display $\delta^{41}K$ values higher than the primitive mantle (Fig. 3), which has a homogeneous potassium isotopic composition with an average $\delta^{41}K$ value of −0.42 ± 0.08‰ (*48*). However, the Mesoproterozoic Grønnedal-Ika carbonatite shows anomalously low $\delta^{41}K$ at −1.84 ± 0.07‰. The Paleozoic and Neoproterozoic carbonatites from Sokli (−0.47 ± 0.06‰ to −0.40 ± 0.06‰) and Fen (−0.44 ± 0.05‰ to −0.30 ± 0.06‰) show mantle-like $\delta^{41}K$ values. The Paleozoic Kovdor samples show variable $\delta^{41}K$ values ranging from −0.63 ± 0.06‰ to 0.13 ± 0.08‰. The Mesozoic carbonatite from Oka (standard COQ-1) shows an average $\delta^{41}K$ of −0.46 ± 0.07‰ (fig. S2). The samples from Jacupiranga (−0.50 ± 0.03‰ to −0.05 ± 0.05‰) and Panda Hill (−0.27 ± 0.04‰) show higher $\delta^{41}K$ values. The Cenozoic continental samples exhibit $\delta^{41}K$ values of −1.20 ± 0.05‰ to −0.46 ± 0.06‰ (Kaiserstuhl), −0.50 ± 0.03‰ to −0.40 ± 0.03‰ (Tororo), and −0.63 ± 0.04‰ (Kerimasi). The Cenozoic oceanic carbonatite from Fuerteventura has mantle-like $\delta^{41}K$ of −0.40 ± 0.05‰, the sample from Fogo Island shows a higher $\delta^{41}K$ value of −0.10 ± 0.04‰, and the two samples from Brava Island show a $\delta^{41}K$ range of −0.78 ± 0.06‰ to −0.04 ± 0.06‰. The natrocarbonatite samples from the active Oldoinyo Lengai volcano have similar $\delta^{41}K$ values irrespective of whether they are fresh (−0.39 ± 0.06‰ to −0.38 ± 0.03‰) or altered (−0.39 ± 0.05‰ to −0.33 ± 0.06‰ for pirssonite-altered samples; −0.44 ± 0.05‰ to −0.36 ± 0.08‰ for calcite-altered samples).

In summary, the investigated carbonatites exhibit a highly variable range of potassium concentrations (46 to 70,092 μg/g) and $\delta^{41}K$ values (−1.84 to 0.17‰). Regardless of location and emplacement age, the carbonatite samples studied show higher and lower $\delta^{41}K$ values relative to primitive mantle composition (Fig. 3).

DISCUSSION

Origins of potassium isotopic signatures in carbonatites

Potassium isotopic fractionation is negligible during mantle partial melting (*47*, *53*). Hence, three main mechanisms may result in potassium isotopic fractionation in magmatic systems subsequent to source extraction, including (i) surface alteration and weathering, (ii) assimilation by continental crustal material, and (iii) magmatic differentiation. We will show that light potassium isotopic compositions of carbonatites can be related to hydrothermal activity, whereas none of the above three processes can account for the extremely high $\delta^{41}K$ values, implying that the heavy potassium isotopic compositions record a source signature.

Weathering and hydrothermal alteration

To assess the impact of weathering and hydrothermal alteration on potassium isotopic fractionation in carbonatites, we collected samples from several well-studied localities: Oldoinyo Lengai (Tanzania), Brava and Fogo islands (Cape Verde), Fen (Norway), Grønnedal-Ika (Greenland), and Kaiserstuhl (Germany). These samples were chosen on the basis of previous detailed fieldwork, petrological studies, and geochemical analyses (*27*, *54*–*57*).

Oldoinyo Lengai is notable as the only active carbonatite volcano and the sole producer of natrocarbonatites. All extrusive carbonatites from this volcano were initially Na rich and later underwent secondary Na-to-Ca substitution processes (*55*, *58*, *59*). To evaluate the potential impact of these substitutions on potassium isotopes, we analyzed a series of natrocarbonatite samples from Oldoinyo

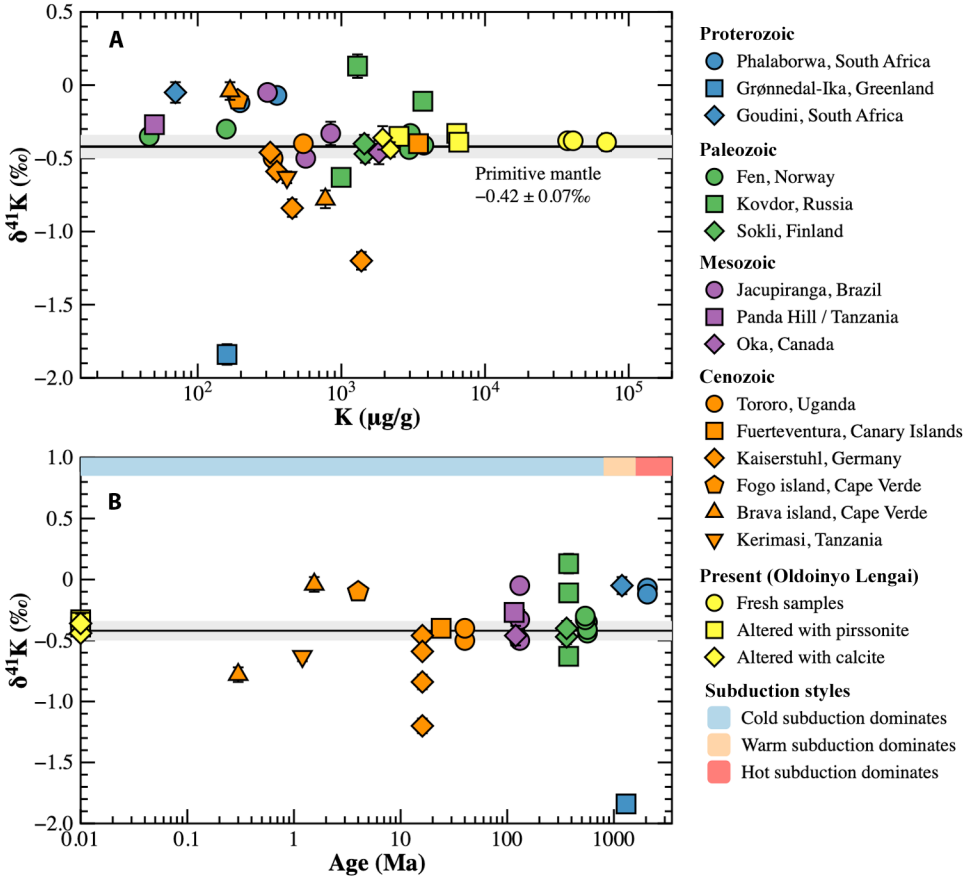

Fig. 3. Potassium isotope systematics of global carbonatites. (**A**) A plot of $\delta^{41}K$ versus potassium content. (**B**) A plot of $\delta^{41}K$ versus age of the investigated carbonatites. Also shown is the summary diagram denoting global geodynamics and slab-top geotherms (*110*). The onset of global plate tectonics at around 3.0 Ga was suggested on the basis of the increasing thickness of juvenile continental crust at this time (*88, 111*). The subduction styles are illustrated using color gradients that represent an evolution from hot subduction (Mesoarchean to Palaeoproterozoic), warm subduction (Palaeoproterozoic to Neoproterozoic) to cold subduction (Neoproterozoic to Phanerozoic). The gray bar shows the $\delta^{41}K$ range of the primitive mantle (*48*). Whole-rock data are used for plotting. In cases where whole-rock data are lacking, carbonate mineral separates (leachates representing the carbonates) were used to proxy for whole-rock compositions, which is a reasonable approach given the similar $\delta^{41}K$ values for whole-rock and carbonate mineral analyses (Fig. 2).

Lengai, ranging from fresh to various degrees of alteration involving pirssonite and calcite. These samples are reported to exhibit large oxygen and carbon isotopic fractionation (typically sensitive to alteration) resulting from hydrothermal processes (fig. S3). Despite noticeable reductions in potassium content due to hydrothermal processes, the altered samples exhibit $\delta^{41}K$ values similar to those of fresh natrocarbonatite (Fig. 3A). The potassium isotopic compositions show no correlation with oxygen or carbon isotopic compositions (fig. S3). This includes two pirssonite carbonatite samples with substantially elevated $\delta^{18}O$ (16.5 and 18.0‰) (*27*) but consistent $\delta^{41}K$ values, indicating limited potassium isotopic fractionation during the Na-Ca substitution processes.

Both an intrusive fresh sample (BRAV-1) and an extrusive altered sample (BRAV-2) of Brava Island in Cape Verde were examined. These samples reveal notable geochemical signals of alteration, as evidenced by their oxygen and carbon isotopic compositions ($\delta^{18}O = 9.06$‰ versus 24.6‰; $\delta^{13}C = -7.49$‰ versus −2.65‰) and fluid-mobile element concentrations {e.g., [Ba] = 26 parts per million (ppm) versus 16050 ppm; [K] = 168 ppm versus 774 ppm} (*27*). The $\delta^{41}K$ values also vary notably between the two samples (−0.04 ± 0.06‰ versus −0.78 ± 0.06‰), with the altered BRAV-2 showing a lighter potassium isotopic composition. Moreover, a fresh carbonatite sample P50 from Fogo Island in Cape Verde displays primary igneous signatures in oxygen and carbon isotopes ($\delta^{18}O = 8.1$‰; $\delta^{13}C = -8.6$‰) (*54*) and a $\delta^{41}K$ value (−0.10 ± 0.04‰) close to that of BRAV-1.

The ferrocarbonatite sample 19781 from Grønnedal-Ika exhibits the lowest $\delta^{41}K$ value observed, likely associated with fluid metasomatism processes, given that the formation of ferrocarbonatite typically involves fluid metasomatism (*60*). The lighter potassium isotopic composition appears to be a general trend for carbonatites influenced by fluid processes, as evidenced by the correlation between $\delta^{41}K$ values and potassium, barium, and rubidium contents observed in Kaiserstuhl samples (fig. S4). In contrast, carbonatite samples from Fen, which have experienced varying degrees of metasomatism by alkali-rich fluids (*27*), show limited $\delta^{41}K$ variation. This observation is particularly noteworthy in the dolomite carbonatite sample P20 (identified as rauhaugite), which occurs in a 20-cm-thick weathering horizon of soil atop the outcrop (*54*). This sample shows the $\delta^{41}K$ comparable to other Fen samples, indicating a lack of substantial potassium isotopic fractionation during alteration processes.

The effects of weathering and hydrothermal alteration on carbonatites are consistent with findings from studies on continental weathering. The enrichment of isotopically light potassium has been observed in weathered basalts (*61*, *62*) and granites (*63*), as well as in riverine dissolved loads and sediments (*64*). This fractionation reflects the preferential incorporation of isotopically heavy and light potassium between fluid and solid/mineral phases (*52*, *61*, *63*, *65*). Conversely, saprolites from an investigated diabase profile display no observable potassium isotopic fractionation, attributed to the conservative behavior of potassium isotopes during diabase weathering (*63*). The observations of carbonatites from Oldoinyo Lengai and Fen are likely analogous to those from the diabase profile.

To sum up, it is reasonable to conclude that fluid metasomatism either has no effect on $\delta^{41}K$ or causes lighter potassium isotopic compositions of carbonatites, essentially depending on the nature of the fluid and the involved mineral phases (*63*, *66*). In any case, the heavy potassium isotopic compositions observed in several carbonatite samples cannot be ascribed to fluid metasomatism.

Assimilation of continental crustal material

The average potassium isotopic composition of the upper continental crust (−0.44 ± 0.05‰ $\delta^{41}K$) (*67*) is indistinguishable from that of the mantle. Thus, the $\delta^{41}K$ values of mantle-derived magmas that assimilated felsic materials from the upper continental crust would have remained unchanged. Continental rocks have, however, heterogeneous $\delta^{41}K$ values, being generally more enriched in light potassium isotopes. For example, typical continental sedimentary rocks and granitoids have $\delta^{41}K$ values ranging from −0.74 to −0.22‰ and −0.68 to −0.34‰, respectively (with statistical outliers excluded from Fig. 4). Even if a high-$\delta^{41}K$ continental reservoir is considered, it is evident from Fig. 4 that assimilation of continental rocks cannot explain the high $\delta^{41}K$ values of carbonatites (up to 0.17‰). Furthermore, the parental melts of carbonatites are likely to have elevated potassium contents due to the incompatibility of potassium during low degrees of mantle melting. The low potassium contents of calciocarbonatites are unlikely to be a primary feature of the parental melts but are probably related to the fact that most carbonatites are cumulate rocks that have undergone hydrothermal overprinting. If the carbonatite-forming magmas were originally more K rich, then the potential effects of crustal assimilation during ascent would have been buffered. Therefore, potassium isotopic variability in carbonatites caused by assimilation during magma ascent through the continental crust appears to be limited. This is supported by oceanic samples (BRAV-1 and P50) that lack any contamination from continental crust and exhibit high $\delta^{41}K$ values. Globally, carbonatites show limited contamination by continental crust-derived materials, which is supported by their $^{143}Nd/^{144}Nd$ and $^{176}Hf/^{177}Hf$ ratios deviating from those of the continental crust (fig. S1). The main reasons for the limited contamination of carbonatites are their low magma viscosities and densities, which enable fast ascent to the surface without much interaction with the continental crust (*68*, *69*). This is also in agreement with previous elemental and isotope studies on carbonatites from several oceanic hotspots, which showed only little or no evidence of interactions with the oceanic lithosphere (*70*).

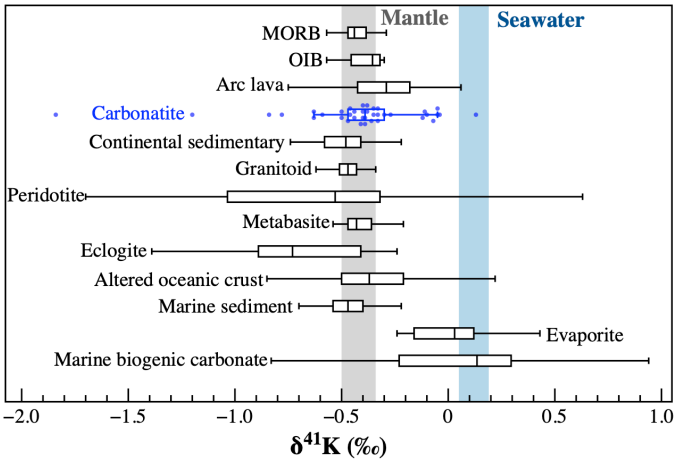

Fig. 4. Compilation of potassium isotopic compositions ($\delta^{41}K$) for carbonatites and other geological materials and reservoirs. The vertical line in the middle of each box represents the median value for each dataset. The width of each box represents the distribution characteristics of 50% of the data, and the vertical lines outside the box represent the minimum and maximum values of each dataset. Except for the carbonatite data, outliers are not shown in the plot for other rock types. Primitive mantle (−0.42 ± 0.07‰) (*48*) and seawater (+0.12 ± 0.07‰) (*78*) are shown for reference. Data sources are listed in table S4.

Magmatic differentiation

Differentiation processes in carbonatite magmatic systems typically occur in three stages: (i) initial fractional crystallization in carbonated silicate magmas until reaching the field of carbonatite-silicate melt immiscibility, (ii) the segregation of carbonatite from silicate melt during immiscibility in the mid-to-lower crust, and (iii) the subsequent crystallization and accumulation of carbonate and noncarbonate minerals to form carbonatite rocks in the upper crust (as illustrated in Fig. 5). To examine the influence of these processes on the $\delta^{41}K$ of carbonatites, we used a simplified petrogenetic model (*71*). We consider the formation of two types of parental melts via low-degree partial melting of the mantle—a CO_2- and CaO-rich melilitite melt (scenario A) and a CaO-poor but MgO-rich melilitite/nephelinite melt (scenario B). In Fig. 5, each scenario traces the evolution of the parental melts, depicting the upward movement indicating decreasing pressure and temperature, which are crucial for silicate-carbonatite immiscibility. The diagrams also outline the relative volumes of different mineral phases that crystallize from these melts. The details for the three differentiation stages are as follows:

(i) Initial fractional crystallization before immiscibility: During this stage, for both parental melt scenarios, the primary crystallized minerals such as olivine, clinopyroxene, perovskite, and magnetite largely exclude highly incompatible potassium and thus do not influence the potassium isotopic compositions of the system. Only minor phases such as nepheline and phlogopite may fractionate potassium and its isotopes. Phlogopite can crystallize in scenarios A and B, whereas nepheline only crystallizes in scenario B.

(ii) Carbonatite-silicate liquid immiscibility: Experimental data and melt inclusion studies [(*71*) and reference therein] suggest that, as temperature and pressure decrease during magma ascent, the CO_2- and CaO-rich melilitite melt may reach the miscibility gap at ~1050° to 1250°C, whereas the CaO-poorer but MgO-richer melilitite/nephelinite melt may undergo silicate-carbonatite melt immiscibility at ~800° to 900°C.

(iii) Crystallization and accumulation of carbonate and noncarbonate mineral phases: After immiscibility, magmatic differentiation of the separated carbonatite melt leads to the crystallization of mainly calcite and apatite, with minor crystallization of olivine, clinopyroxene,

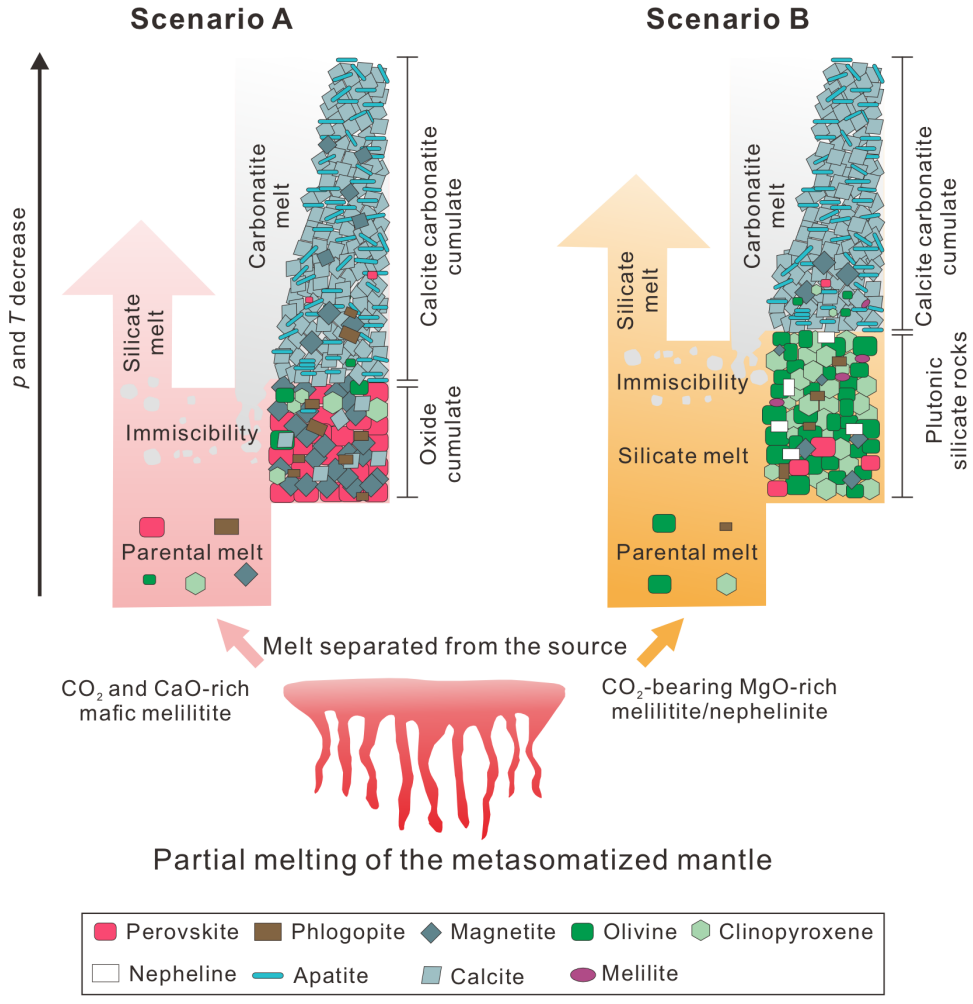

Fig. 5. A schematic diagram showing the paths of parental melts to generate carbonatites. Each scenario portrays the simplified evolution of parental melts, adapted from (*71*) (https://creativecommons.org/licenses/by/4.0/), with the upward direction indicating decreasing pressure (*p*) and temperature (*T*), highlighting the relative conditions under which carbonatite melt separates from the parental melt, resulting in silicate-carbonatite immiscibility. The relative volumes of different crystallized minerals are indicated. The diverse parental melts are generated through the partial melting of distinct source rocks. The CO_2- and CaO-rich melilitite melt demonstrates the capability to reach immiscibility at higher pressures and temperatures, contrasting with a CaO-poorer but MgO-richer melilitite/nephelinite melt, which exhibits silicate-carbonatite immiscibility at lower pressures and temperatures.

perovskite, melilite, and phlogopite. Among these liquidus phases, phlogopite is the only one containing stoichiometric potassium (scenario A).

In this study, we quantitatively modeled the potassium isotopic fractionation occurring during fractional crystallization and immiscibility processes in carbonatite systems. A crucial parameter in this modeling is the fractionation factor between K-bearing minerals and melts, which must be confidently constrained. Considering that the K—O bond length in silicate glass (3.00 to 3.06 Å) is close to that in microcline (2.94 Å) (*72*), the fractionation factor $\Delta^{41}K_{carbonate\text{-}microcline}$ is used as an approximation of $\Delta^{41}K_{carbonatite\ melt\text{-}silicate\ melt}$. Carbonatite melts are ionic liquids consisting of CO_3^{2-} molecular anions and metal cations (*73*). We used the theoretical fractionation factor for different potassium carbonates (potassium carbonate, K_2CO_3; potassium bicarbonate, $KHCO_3$; hydrated potassium carbonate, $K_2CO_3{\cdot}1.5H_2O$) and microcline (*51*). Thus, on the basis of first-principles calculations (*51*), equilibrium potassium isotopic fractionation between carbonate and silicate minerals is expected to be small at magmatic temperatures, with slight preferential incorporation of the heavy isotopes of potassium into carbonates.

To validate these theoretical calculations, we conducted chemical leaching experiments on carbonatite samples (details in Materials and Methods). Selective dissolution experiments revealed that most potassium is hosted within carbonates, with $\Delta^{41}K_{carbonate\text{-}bulk}$ ($\delta^{41}K_{carbonate} - \delta^{41}K_{whole\text{-}rock}$) values being close to zero within uncertainties (Fig. 2). Exceptions were observed for four samples—P23, 19781, U73, and BRAV-2—where the $\Delta^{41}K_{carbonate\text{-}bulk}$ values are slightly above zero (Fig. 2). Our experiments confirm that equilibrium potassium isotopic fractionation primarily occurs between carbonate and silicate minerals and that the observed isotopic fractionation is limited. The positive $\Delta^{41}K_{carbonate\text{-}bulk}$ offsets may, to some extent, reflect the preferential incorporation of heavy potassium isotopes into

carbonate minerals. These findings are consistent with the first-principles calculations in (*51*), supporting the use of theoretical fractionation factors in our quantitative modeling.

Nepheline preferentially incorporates heavy potassium isotopes relative to silicate melt (*51*). Its early crystallization results in only minor negative shifts in $\delta^{41}K$ (fig. S5), which cannot account for the elevated $\delta^{41}K$ values observed in carbonatites. In contrast, because of the preferential incorporation of light potassium isotopes (*51*), the crystallization of phlogopite could result in residual melts with heavier potassium isotopic compositions (*74*). We simulated the potassium isotopic evolution during fractional crystallization of phlogopite (stages i and iii) using the following equations

$$\delta^{41}K_{melt} = \delta^{41}K_{initial\ melt} + \Delta^{41}K_{crystal-melt} \times \ln(f_K)$$

$$\Delta^{41}K_{mineral-melt} = 1000 \times \ln(\alpha_{mineral-melt})$$

$$f = \frac{F}{F + D \times (1-F)}$$

where $\delta^{41}K_{initial\ melt}$ is the potassium isotopic composition of initial magmas, and $\delta^{41}K_{melt}$ represents the potassium isotopic composition of magmas which is produced when initial magmas experience crystal fractionation. f is the fraction of potassium in the residual melt. F is the degree of fractional crystallization. $\Delta^{41}K_{mineral-melt}$ is the isotopic fractionation factor for mineral-melt pairs. The potassium isotopic fractionation factors can be calculated following theoretical considerations (*51*). D is the partition coefficient; a value of ~3.67 is applied for phlogopite (*75*). Considering the generation of cumulates of mafic silicate and oxide minerals ± phlogopite during stage i, we set $\delta^{41}K_{initial\ melt} = \delta^{41}K_{melt}$ (previous step). This approach models the scenario where phlogopite (as a cumulate) is removed from the system in an incremental batch removal mode (assumed 5 and 10%, respectively) during fractional crystallization. For stage iii, where only a limited amount of phlogopite crystallizes, our modeling adopts the continuous removal of phlogopite.

Our modeling demonstrates negligible isotopic shifts in $\delta^{41}K$ during phlogopite crystallization from the silicate melt at 1000° to 1200°C (stage i) for both parental magma scenarios, even under conditions of high degrees of crystallization (Fig. 6A). In contrast, the modeling suggests that phlogopite crystallization from carbonatite melts at 900° to 1100°C (stage iii) could lead to more pronounced $\delta^{41}K$ shifts (Fig. 6B). However, magnesium in the system preferentially forms minerals like olivine and pyroxene, reducing the amount of phlogopite that crystallizes. Consequently, with a realistic proportion of phlogopite (e.g., <30%), the $\delta^{41}K$ shift remains limited to less than 0.05‰, which is minor. These results align with our chemical leaching experiments, which showed that even when silicate minerals (primarily phlogopite) account for more than 50% of potassium in the system, $\Delta^{41}K_{carbonate\text{-}bulk}$ remains near zero (Fig. 2). Therefore, crystallization processes cannot explain the extremely heavy potassium isotopic compositions observed in some carbonatites.

We also modeled carbonatite-silicate melt immiscibility (stage ii) at temperatures of 1050° to 1250°C for scenario A and 800° to 900°C for scenario B. The results suggest that potassium isotopic fractionation during immiscibility at equilibrium fractionation is negligible (Fig. 7). If given Rayleigh fractionation, liquid immiscibility could result in evolved silicate melts and conjugate carbonatite liquids that may have extremely light potassium isotopic compositions compared to the parental magmas. Liquid immiscibility potentially results in $\delta^{41}K$ shifts of up to ~0.06‰ in pooled carbonatite melts for scenario A and up to 0.09‰ for scenario B (Fig. 7). These $\delta^{41}K$ shifts are minor. The natrocarbonatite samples from Oldoinyo Lengai

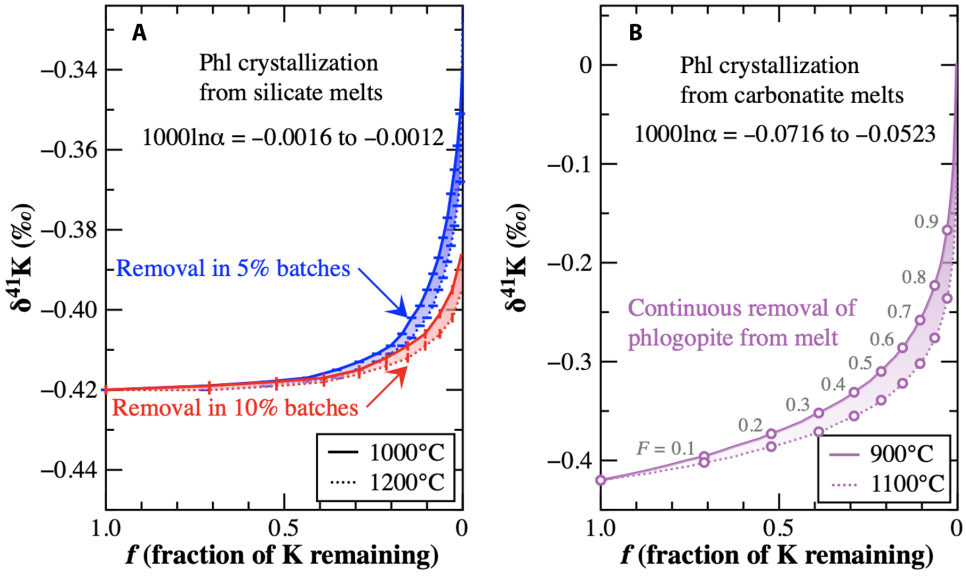

Fig. 6. Diagrams documenting potassium isotopic variation of melts during the crystallization of phlogopite. The fractionation factor α refers to the ratio of $^{41}K/^{39}K$ between phlogopite and microcline (*51*). (**A**) Phlogopite fractionation from parental melts at 1000° to 1200°C (scenarios A and B), in which phlogopite (as the form of cumulates olivine + clinopyroxene + perovskite + magnetite + phlogopite; Fig. 5) is removed from the system in discrete batches. (**B**) Phlogopite crystallization from carbonatite melts at 900° to 1100°C (scenario A), in which phlogopite is modeled to be continuously removed from the system. For more details on modeling, see the main text.

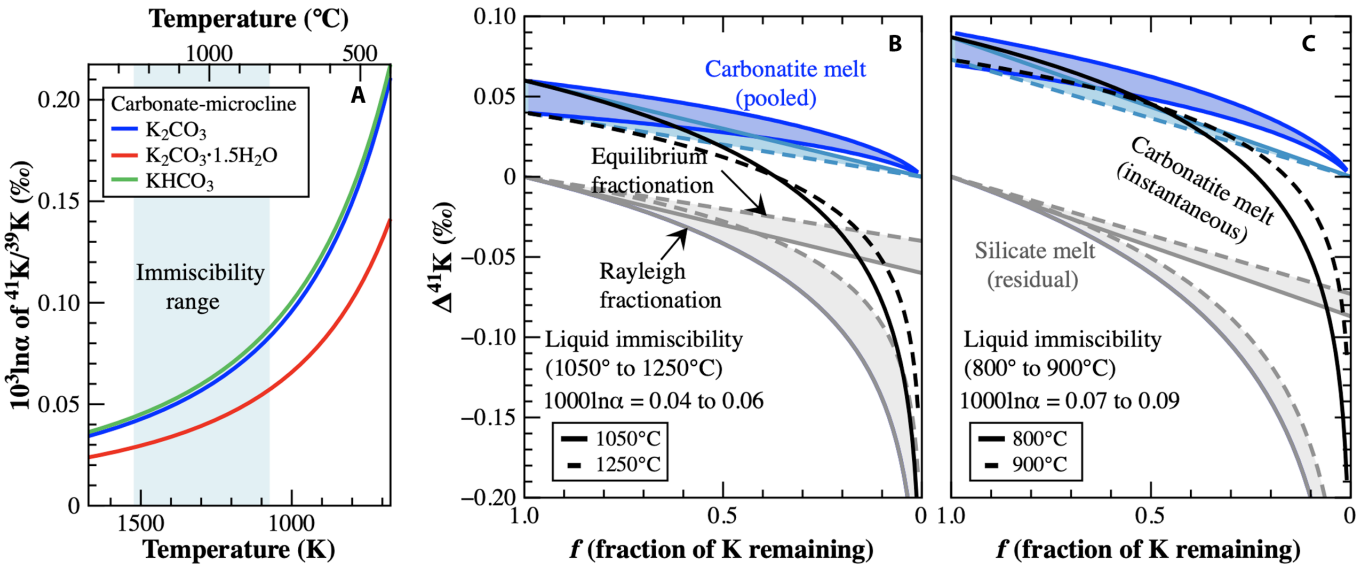

Fig. 7. Diagrams modeling potassium isotopic fractionation during liquid immiscibility. (**A**) First-principles calculation of potassium isotopic fractionation as a function of temperature between different potassium carbonates (potassium carbonate, K_2CO_3; potassium bicarbonate, $KHCO_3$; hydrated potassium carbonate, K_2CO_3·1.5H_2O) and silicates (represented by microcline) (*51*), where the fractionation factor α refers to the ratio of $^{41}K/^{39}K$ between carbonate and microcline. The blue area shows the calculated equilibrium potassium isotopic fractionation for carbonate-silicate melt immiscibility from 800° to 1250°C. The gray area shows the results for a relatively high potassium loss ratio, ranging from 50 to 80%. (**B** and **C**) Models of potassium isotopic variation during equilibrium fractionation and Rayleigh fractionation for carbonatite-silicate melt immiscibility at various temperatures.

support this observation. These natrocarbonatites, argued to be formed by immiscibility from a nephelinite parent magma at upper crustal pressures (*76*), still exhibit mantle-like $\delta^{41}K$ values (Fig. 3), demonstrating the limited impact of immiscibility on their potassium isotopic compositions.

To summarize, the combined modeled effects of magmatic differentiation in carbonatite systems can explain the slight positive offset observed for several carbonatite samples. However, magmatic differentiation cannot account for the higher $\delta^{41}K$ observed for samples from Phalaborwa, Goudini, Kovdor, Jacupiranga, and Cape Verde. These heavy potassium isotopic compositions are most likely inherited from mantle sources.

Carbonate-rich oceanic crust in the mantle sources of carbonatites

The potassium isotopic compositions in the mantle sources of some carbonatites are heavier than the primitive mantle estimate and the mid-ocean ridge basalts (MORBs) and OIBs analyses but fall in the range of oceanic materials such as AOC and marine carbonates (Fig. 4). Potassium is enriched in fluids/melts derived from the devolatilization or remelting of AOC and sediments. Therefore, metamorphic processes accompanying slab burial are expected to affect the potassium isotopic composition of both the metasomatized mantle and the residual slab (*44*, *45*, *50*). Mantle-derived xenoliths from cratonic regions affected by ancient subduction-related metasomatism may exhibit elevated $\delta^{41}K$ values in phlogopite (e.g., +0.2 to +0.6‰) (*53*), reflecting the isotopic signature of past slab-derived components.

Recent analyses of potassium isotopes in arc volcanic rocks demonstrate a variation in $\delta^{41}K$ values, encompassing both lower and higher $\delta^{41}K$ values than those typical of the mantle (Fig. 4). Given the preferential incorporation of heavy potassium isotopes into fluids during slab dehydration (*65*), the heavy potassium isotopic composition in arc lavas was attributed to the addition of heavy potassium from slab-derived fluids ($\delta^{41}K$ up to 1.4‰) in their sources (*45*, *50*). This effect is predominant at a forearc depth but diminishes at the rear-arc mantle (*50*). Moreover, it remains uncertain whether dehydration-related fractionation of carbonated oceanic crusts can substantially alter the potassium budget of the residual slab and its $\delta^{41}K$ signature. For instance, a study of eclogites from Sumdo, Tibet revealed large variations in $\delta^{41}K$, ranging from −1.64 to −0.24‰ (*65*); whereas MORB-like $\delta^{41}K$ values were observed in subducted metabasites (reaching up to lawsonite-blueschist facies) exhumed from serpentinite mud volcanoes in the Mariana forearc (Fig. 4) (*77*). Furthermore, if slab-derived fluids were responsible for the heavy potassium isotopic signatures in carbonatites, then these signatures would then be expected to be prevalent in Phanerozoic carbonatites associated with cold subduction zones, where fluid release is common. In contrast, ancient carbonatites that formed in settings of warm or hot subduction are more likely to reflect slab melting rather than fluid release. The high $\delta^{41}K$ values observed in the Phalaborwa (~2060 Ma) and Goudini (~1190 Ma) carbonatites do not support the hypothesis of a fluid-dominant contribution.

Subducted sediments represent important potassium reservoirs of the subducting slab; however, typical sediments do not show $\delta^{41}K$ values as high as what is observed in carbonatites (Fig. 4). In general, silicate sediments exhibit low $\delta^{41}K$ values (down to −1.3‰) (*41*), reflecting continental input, as low-$\delta^{41}K$ detrital components control the potassium budget. Loss of heavy ^{41}K during continental weathering generates low-$\delta^{41}K$ signatures in continent-derived materials (*63*). In contrast, as seawater has high $\delta^{41}K$ values (e.g., +0.12 ± 0.07‰) (*78*), marine authigenic minerals precipitated from seawater such as marine evaporites and carbonates would inherit high $\delta^{41}K$ from seawater (Fig. 4). Alternatively, these minerals precipitated from a fluid enriched in ^{41}K (e.g., a MOR hydrothermal fluid that had equilibrated

with evaporated seawater or crystallized sylvite). Nevertheless, subduction of pure carbonate sedimentary is likely to have limited influence on the $\delta^{41}K$ of the mantle for two reasons. First, carbonate minerals typically contain very low potassium content. Second, subducted sediments are generally low in carbonate minerals as they are deposited below the carbonate compensation depth (*6*). Moreover, although ophicarbonates have been proposed to be a source of carbon (*8*, *9*), they are unlikely to be an important source of potassium transferred to the deep Earth, given their low potassium contents. In comparison, AOCs, especially in the upper 600 m of oceanic crust, have high proportions of authigenic silicate and carbonate minerals (*10*, *11*). They provide important sources of CO_2, calcium, potassium, and strontium for mantle metasomatism (*3*, *70*). If these authigenic minerals resist decarbonization and dehydration in subducting slabs, then they could be transferred to the mantle sources of carbonatites, leading to high $\delta^{41}K$ in metasomatized mantle domains. A recent study suggests that such heavy potassium isotopic signatures also characterized the Archean AOC (*79*).

We tested the slab recycling hypotheses using Monte Carlo simulation, assuming that potassium element exchange and isotopic variation are solely based on mass balance. The simulation follows

$$[K]_M = [K]_A \times f + [K]_B \times (1-f)$$

$$\delta^{41}K_M = \delta^{41}K_A \times f \times ([K]_A/[K]_M) + \delta^{41}K_B \times (1-f) \times ([K]_B/[K]_M)$$

where A and B are two mixing endmembers and M represents the mixture; [K] represents the potassium concentration; $\delta^{41}K$ refers to potassium isotopic composition; f refers to the mixing ratio ($0 \leq f \leq 1$). Four combinations are used in the simulation, involving the mixing of MORBs with carbonate sedimentary (to model the compositions of carbonated AOC) and the mixing between mantle and sediment, eclogite, and carbonated AOC. Each combination was simulated with 10,000 trials. Random numbers were attributed to f. Only simulations with $f \leq 0.3$ were considered realistic. Our simulations use randomly assigned endmember compositions, following a normal distribution (mean ± 1 SD) based on reported $\delta^{41}K$ data for each endmember. Modeling parameters are provided in table S5. Our modeling for carbonated AOC yielded an average $\delta^{41}K$ of −0.29 ± 0.13‰ (Fig. 8A).

Simulation results indicate that subducted sediments or recycled eclogite components can generate mantle heterogeneities primarily characterized by either unchanged or lighter potassium isotopic compositions (Fig. 8C). In the case of sediments, this is because the potassium abundance and isotopic composition of subducting sediments are primarily controlled by continent-derived detrital materials rather than marine authigenic components (*41*). Weathering and erosion of the continental crust produce low $\delta^{41}K$ signatures (*61*, *63*, *64*). Consequently, the lighter potassium isotopic signatures in these sediments, contrasting with the heavy potassium isotopic composition observed in our samples, imply a limited influence of recycled continent-derived materials on the potassium isotopic budget of the mantle sources to carbonatites.

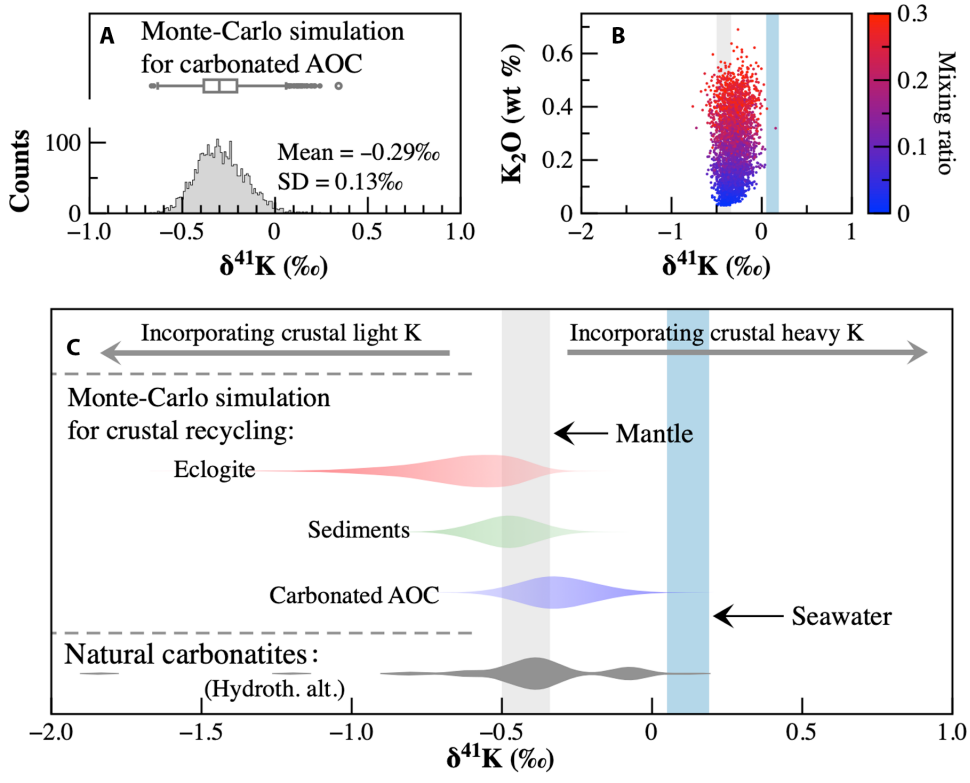

Fig. 8. Diagrams of Monte-Carlo simulations. (**A**) The normal distribution of modeled potassium isotopic compositions of carbonate-rich oceanic crusts based on Monte Carlo simulation. (**B**) The modeled compositions of mantle sources metasomatized by recycled carbonated AOC at variable mixing ratios of 0 to 30%. (**C**) Violin plots of potassium isotopic data of carbonatite samples and the Monte-Carlo simulation results of mantle mixing with eclogite, subducting sediments, and carbonated AOC, respectively (details on modeling are in the main text). Extremely light potassium isotopic composition in carbonatites is generated by fluid metasomatism.

Conversely, our modeled mantle, which was metasomatized by carbonated AOC at variable mixing ratios (0 to 30%), exhibits highly variable $\delta^{41}K$ values, ranging between those of the mantle and seawater (Fig. 8B). This variability largely stems from the complex formation processes of AOC, which likely contribute to their diverse potassium isotopic compositions (*41*, *46*, *80*). Observations from natural carbonatite samples align with this modeled range of $\delta^{41}K$, indicating the influence of carbonated AOC. Notably, even at high mixing ratios (e.g., >20%), the recycling of carbonated AOC can yield $\delta^{41}K$ values matching typical mantle signatures (Fig. 8B). Therefore, mantle-derived magmas with mantle-like $\delta^{41}K$ values do not necessarily exclude the influence of carbonated AOC in their source. Consequently, the potassium isotopic compositions of the mantle sources of carbonatites are likely highly heterogeneous; not all carbonatites will exhibit elevated $\delta^{41}K$ values despite potentially substantial contributions from carbonated AOC. Integrating additional isotopic systems into the information retrieved from potassium isotopes is essential for resolving this ambiguity. However, those carbonatites with high $\delta^{41}K$ must have been derived from mantle sources that contained recycled oceanic crust.

Two possible mechanisms may explain the heterogeneous potassium isotopic compositions in carbonatite sources. Subducted oceanic crusts, varying in lithologies (i.e., mineral assemblages and chemical compositions) and $\delta^{41}K$ values may contribute to the metasomatism of the mantle that is heterogeneous on the temporal and regional scale. As a result, the metasomatized mantle domains exhibit highly variable but relatively heavy potassium isotopic compositions (Fig. 8B). Alternatively, heterogeneous potassium isotopic signatures in carbonatites may reflect the superposition of multiple additions from subducted slabs. Different events could substantially increase the amounts of subducted material in the mantle sources. In particular, given that subducted slabs can penetrate deep into the lowermost mantle and reach the core-mantle boundary (*81*), plumes formed at this boundary may effectively transport subducted crustal carbon to the surface or interact with a previously metasomatized lithospheric mantle (*3*, *82*). Thus, external-derived carbon in the sources of carbonatites likely originates from multiple slabs and may even involve ancient oceanic crusts.

Oceanic crust subduction–driven deep carbon cycle

Since carbonatites are products of carbon-rich melts derived from the Earth's upper mantle, their geochemical signatures (including potassium isotopes) offer valuable insights into deep carbon cycling; i.e., whether carbon and associated volatiles in their mantle sources are primordial or recycled. If the mantle sources of carbonatites contain recycled crustal carbon, then recycled potassium is most probably also present. Carbonates were likely present on the ocean floor as early as the Eoarchean (>3.65 Ga) (*83*). Components of oceanic crusts have been available for mantle metasomatism and enrichment since the Archean (*84*, *85*). Recent studies using calcium isotopes suggest that carbonates were incorporated into the sources of tonalite-trondhjemite-granodiorite suites, supporting the subduction-driven carbon recycling during the Archean (*86*). However, before ~1.6 Ga, high-degree melting in globally hot subduction zones resulted in low retention of carbonates in subducting slabs, thereby limiting the deep carbon cycle (*87*). As the Earth's mantle cooled, Meso- to Neoproterozoic warm subduction zones and Phanerozoic cold subduction zones facilitated the transfer of carbonates beyond the depth of arc-magma generation into the deeper mantle (*88*–*91*). Although no variation of $\delta^{41}K$ in carbonatites over time was observed in our samples, evidence from Mesoproterozoic to Cenozoic high-$\delta^{41}K$ carbonatites (Fig. 3B) supports that both cold and warm subduction processes enabled the introduction of marine carbonates into the mantle. Besides, both oceanic and continental carbonatite samples exhibit heavy potassium isotopic signals related to recycled carbonates. Thus, we propose that carbonate materials in carbonatite sources may originate from a deep-rooted mantle plume carrying the high $\delta^{41}K$ signature from the lower mantle (e.g., OIB-like carbonatites) or from the interaction between the mantle plume and a carbonated lithospheric mantle, where carbonatite magmas were produced through low-degree melting. In either case, marine carbonates were transferred into the mantle via the recycling of carbonate-rich AOC, supporting the notion that oceanic crust subduction has been an effective mechanism for the deep carbon cycle.

Notably, the Kaapvaal craton in South Africa provides valuable insights. The Archean carbonate-rich eclogites have been found in the kimberlites from Kaapvaal, which reflected the recycling of ancient oceanic crust in the mantle beneath Kaapvaal (*92*). The Phalaborwa carbonatites (~2.06 Ga) from the Kaapvaal craton exhibit high $\delta^{41}K$ values (Fig. 3), supporting the addition of carbonate material. This conclusion aligns with previous calcium isotope studies of these carbonatites (*28*). In addition, the Phalaborwa carbonatites display unique mass-independent sulfur isotopic signatures ($\Delta^{33}S$ values = 0.2 to 0.7‰; Fig. 9) (*93*). This reflects the influence of Archean sedimentary rocks known for mass-independent sulfur isotopic fractionation ($\Delta^{33}S \neq 0$) due to atmospheric photodissociation before the Great Oxidation Event (GOE; ~2.4 Ga) (*94*). Anomalous $\Delta^{33}S$ signals have also been observed in some OIBs (*95*, *96*), with these anomalies linked to hydrothermal processes in the Archean basaltic crust, during which sedimentary mass independent fractionation-sulfur (MIF-S) was recycled into the upper hydrated

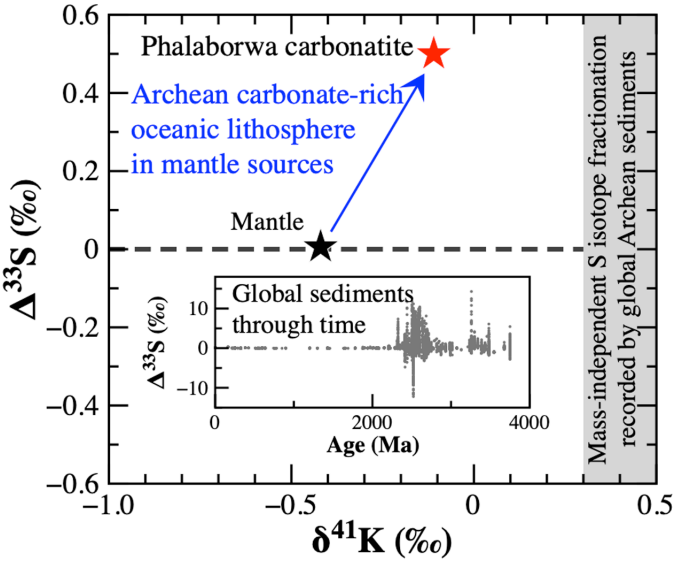

Fig. 9. A plot of $\delta^{41}K$ versus $\Delta^{33}S$ of the carbonatite (~2.06 Ga) from Phalaborwa, South Africa. The $\Delta^{33}S$ value of the carbonatite from Phalaborwa is from (*93*). The small plot inside shows the $\Delta^{33}S$ variation of the global sediments through time. Most of the mass-independent fractionation of sulfur isotopes ($\Delta^{33}S \neq 0$) was observed in sediments before the GOE at ~2.45 Ga (*94*). The full data of global sediments are from the available database published in (*112*).

oceanic crust (*95*). The subsequent subduction of MIF-S bearing AOC likely facilitated the recycling of these sulfur isotopic signatures into deep mantle sources, ultimately manifesting in some OIBs. Drawing from this, a similar process could explain the observed MIF-S and heavy potassium isotopic signatures observed for the Phalaborwa carbonatite. Therefore, distinctive potassium, calcium, and sulfur isotopic signals in the Phalaborwa carbonatites collectively confirm the contribution of the Archean carbonated oceanic lithosphere to the mantle sources of carbonatites (*93*). This finding implies that despite the potential melting of carbonate rocks in Archean hot subducted slabs, residual carbonate may have been sequestered in downwelling slabs, at least locally, and eventually transferred to the deep Earth. Thus, the initiation of effective crustal carbon transfer into the deep Earth could be dated back to the Archean. Our results highlight the mantle's capacity to serve as an important reservoir of crustal carbon since the Archean, initiated by the onset of oceanic lithosphere subduction. Thus, oceanic crust subduction could have played a crucial role in moderating atmospheric pCO_2 levels throughout Earth's history.

The genesis of carbonatites associated with plate subduction

As previously mentioned, the Goudini (~1190 Ma) and Phalaborwa (~2060 Ma) carbonatites may reflect tectonic activity linked to warm or hot subduction zones (Fig. 10A), where carbon bypasses shallow degassing and enters into the deep Earth. This process could have become more prevalent during the Phanerozoic, characterized by cold subduction zones. The rise in biogenic carbon since the Cambrian Explosion (~550 Ma) likely influenced this process (*6*, *97*). Phanerozoic carbonatites (<540 Ma) exhibit variations in boron and strontium isotope compositions (*20*, *23*). These isotopic shifts might be related to substantial changes in the mantle composition that produced these carbonatites, associated with the onset of modern-style subduction. Evidence comes from the steady increase in $\delta^{11}B$ values in marine carbonates since the Silurian (Fig. 10B) (*98*), suggesting a boron cycle that was influenced by plate tectonics and biosphere evolution. This trend is also reflected in strontium isotopes; increasing $^{87}Sr/^{86}Sr$ ratios in marine carbonates over time indicate more radiogenic strontium recycling into the mantle (*99*), as supported by strontium isotope trends in global carbonatites that are equivalent to those of seawater (Fig. 10C). Potassium isotopes offer an additional avenue for tracing subducted components. Marine biogenic carbonates exhibit high $\delta^{41}K$ values similar to seawater (Fig. 4), indicating the potential of potassium isotopes to trace such recycling. Although our dataset is limited, heavy potassium isotopic compositions have been observed in Phanerozoic carbonatites (e.g., Kovdor, Jacupiranga, and Cape Verde), which are likely inherited from seawater, analogous to the message from strontium data. These results reflect that the mantle sources of carbonatites have been increasingly affected by subduction. It is also important to note that boron strongly partitions into aqueous fluids at relatively low temperatures and pressures (e.g., during pore water expulsion and clay breakdown in subducting sediment), causing most boron to be stripped from the oceanic slab before contributing significantly to arc magmatism (*100*). By contrast, potassium is retained in high-pressure minerals such as phengite or omphacite (*101*), which can remain stable to >100-km depths in residual slabs, experiencing only minor losses in localized high–fluid flux zones. Thus, a subducted slab can preserve a strong potassium isotopic fingerprint of recycled surface materials.

Subduction events may have also influenced the deep mantle, facilitating the recycling of subducted materials through plume activity. For example, studies of young oceanic carbonatites from Fuerteventura and Cape Verde have reported a range of elemental and isotopic compositions (carbon, oxygen, strontium, neodymium, lead, helium, neon, and argon) [summarized in (*102*)].

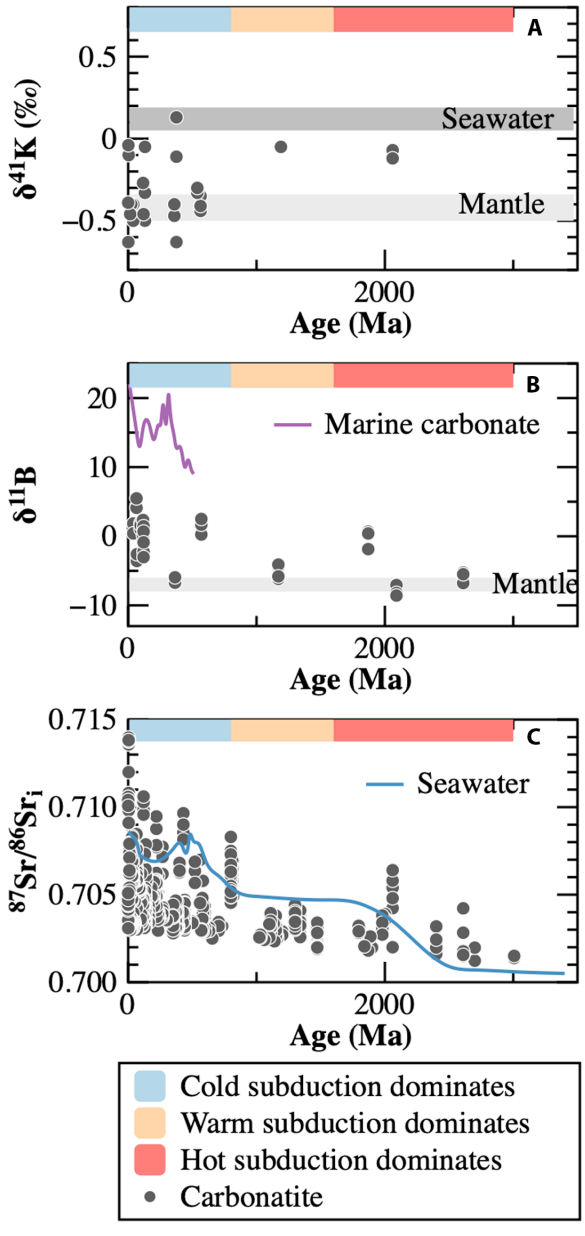

Fig. 10. Evolution diagrams for potassium, boron, and strontium isotopic compositions of global carbonatites. The main data sources: for (**A**), this study (samples of which potassium isotopic compositions are substantially modified by alteration are excluded); for (**B**), (*23*); and for (**C**), (*20*, *99*). The subduction styles are illustrated using color gradients that represent an evolution from hot subduction, warm subduction, to cold subduction.

The most notable difference between these carbonatites is their He isotopic compositions: Fuerteventura displays a shallow lithospheric mantle signature, whereas Cape Verde shows a deep lower mantle signature (*102*). Potassium isotopes provide further constraints. The carbonatite from Fuerteventura shows a $\delta^{41}K$ value of -0.40 ± 0.05‰, whereas those from Cape exhibit higher $\delta^{41}K$ values of -0.10 ± 0.04‰ and -0.04 ± 0.06‰, indicative of carbonated AOC signatures. Recent research on the Madeira OIBs suggests that potassium and its isotopic signature of the upper oceanic crust can undergo subduction into the deep mantle and subsequently be recycled back to the surface via mantle plumes (*103*). Thus, potassium isotopic data, in combination with helium isotopes, support a scenario in which carbonated oceanic crust is subducted into the deep mantle, and the subducted material later contributes to the mantle source of Cape Verde carbonatites via plumes (*70*).

In contrast, the modern natrocarbonatites from Oldoinyo Lengai display potassium isotopic compositions within the mantle range. While Sr-Nd-Pb isotope data point to a range of involved mantle reservoirs, including an enriched mantle component (EM1), the homogeneous isotopic signatures of carbon, oxygen, lithium, and barium indicate a dominant mantle contribution with limited evidence for recycled crustal components (*59*, *104*, *105*). This suggests a homogeneous mantle source (in terms of stable isotopes) where any potential crustal influence is effectively diluted. Consequently, as shown in previous studies and by our data, the formation of Na-rich carbonatites at Oldoinyo Lengai may not require an exceptionally carbon-rich mantle; instead, these carbonatites are likely generated in the shallow crust via immiscibility from silicate magmas (*76*).

MATERIALS AND METHODS

The investigated carbonatites ($n = 38$) were sampled from 14 locations (Fig. 1), including 1 to 2060 Ma continental carbonatites from Africa (Phalaborwa, Goudini, Panda Hill, Tororo, and Kerimasi), Germany (Kaiserstuhl), Norway (Fen), Finland (Sokli), Russia (Kovdor), Greenland (Grønnedal-Íka), Brazil (Jacupiranga), and Canada (Oka) and 0.3 to 24 Ma carbonatites from the oceanic hotspots of Canary Islands (Fuerteventura) and Cape Verde (Fogo and Brava), as well as recent natrocarbonatites from Oldoinyo Lengai. Detailed information on samples is documented in tables S1 and S2.

Chemical and isotopic measurements were conducted at the Institut de Physique du Globe de Paris (IPGP). For each sample, ~15 mg of a homogenized bulk powder was dissolved using 0.5 M HNO_3 (2 ml) in polytetrafluoroethylene beakers at room temperature for ~24 hours. The solutions were then centrifuged to separate carbonate solutions from any remaining silicate and oxide particles. Solutions of carbonate were subsequently evaporated to dryness and redissolved in 0.5 M HNO_3 for column chemistry (carbonate separate group), and the remaining residues were discarded. To further investigate the effect of the silicate and oxide, we also dissolved the bulk powders, in instances where a high proportion of solid residues were observed after dissolution. To minimize the formation of fluorides, we first separated the carbonate minerals using 0.5 M HNO_3 and centrifugation. The remaining solids were then further dissolved using a mixture of concentrated HNO_3 (500 μl) and hydrofluoric acid (HF; 1.5 ml), followed by heating at 120°C for ~48 hours. After evaporating the HNO_3:HF mixture, the residues were treated with a mixture of concentrated HCl (1.5 ml) and HNO_3 (500 μl) and heated to dissolve any remaining fluoride complexes. Last, the mixed solutions containing carbonate and silicate + oxide (bulk group) were evaporated to dryness and redissolved in 0.5 M HNO_3 for subsequent experiments.

Sample solutions were loaded onto Bio-Rad Poly-Prep columns filled with 2 ml of Bio-Rad AG 50 W-X8 cation exchange resin (200 to 400 mesh). Four passes of column chemistry were performed for both standards and carbonatite samples. More details on chemical purification and analytical procedures were described earlier in (*106*, *107*). The potassium concentration and isotopic compositions were determined using a Nu Sapphire collision-cell multicollector inductively coupled plasma mass spectrometer. Isotopic ratios were measured using the standard-sample-standard bracketing method, and potassium isotopic compositions are expressed using delta notation relative to the standard [National Institute of Standards and Technology (NIST) Standard Reference Material (SRM) 3141a] as follows: $\delta^{41}K\ (‰) = [(^{41}K/^{39}K_{sample}/^{41}K/^{39}K)_{standard} - 1] \times 1000$. Isotopic analytical uncertainties are reported as 2 SD. Terrestrial standards BHVO-2 and AGV-2 yield $\delta^{41}K$ values of -0.42 ± 0.04‰ (2 SD; $n = 7$) and -0.50 ± 0.03‰ (2 SD; $n = 7$), respectively, which agree with published results (*106*–*109*). Our study also presents the first $\delta^{41}K$ measurement for the carbonatite standard COQ-1, which was determined to be -0.46 ± 0.07‰ (2 SD; $n = 48$; fig. S2) and may serve as a reference value for future studies.

Supplementary Materials

This PDF file includes:

Figs. S1 to S5
Tables S1 to S5
References

REFERENCES AND NOTES

1. M. W. Broadley, P. H. Barry, C. J. Ballentine, L. A. Taylor, R. Burgess, End-Permian extinction amplified by plume-induced release of recycled lithospheric volatiles. *Nat. Geosci.* **11**, 682–687 (2018).
2. R. Dasgupta, M. M. Hirschmann, The deep carbon cycle and melting in Earth's interior. *Earth Planet. Sci. Lett.* **298**, 1–13 (2010).
3. S. F. Foley, T. P. Fischer, An essential role for continental rifts and lithosphere in the deep carbon cycle. *Nat. Geosci.* **10**, 897–902 (2017).
4. F. Zhang, S. Xiao, B. Kendall, S. J. Romaniello, H. Cui, M. Meyer, G. J. Gilleaudeau, A. J. Kaufman, A. D. Anbar, Extensive marine anoxia during the terminal Ediacaran Period. *Sci. Adv.* **4**, eaan8983 (2018).
5. M. M. Hirschmann, Comparative deep Earth volatile cycles: The case for C recycling from exosphere/mantle fractionation of major (H_2O, C, N) volatiles and from H_2O/Ce, CO_2/Ba, and CO_2/Nb exosphere ratios. *Earth Planet. Sci. Lett.* **502**, 262–273 (2018).
6. T. Plank, C. E. Manning, Subducting carbon. *Nature* **574**, 343–352 (2019).
7. T. Plank, *The Chemical Composition of Subducting Sediments in Treatise on Geochemistry (Second Edition)*, H. D. Holland, K. K. Turekian, Eds. (Elsevier, 2014), pp. 607–629.
8. D. M. Kerrick, J. A. D. Connolly, Subduction of ophicarbonates and recycling of CO_2 and H_2O. *Geology* **26**, 375–378 (1998).
9. J. Eguchi, R. Dasgupta, Cycling of CO_2 and H_2O constrained by experimental investigation of a model ophicarbonate at deep subduction zone conditions. *Earth Planet. Sci. Lett.* **600**, 117866 (2022).
10. H. Staudigel, S. R. Hart, Alteration of basaltic glass: Mechanisms and significance for the oceanic crust-seawater budget. *Geochim. Cosmochim. Acta* **47**, 337–350 (1983).
11. J. C. Alt, D. A. H. Teagle, The uptake of carbon during alteration of ocean crust. *Geochim. Cosmochim. Acta* **63**, 1527–1535 (1999).
12. P. B. Kelemen, C. E. Manning, Reevaluating carbon fluxes in subduction zones, what goes down, mostly comes up. *Proc. Natl. Acad. Sci. U.S.A.* **112**, E3997–E4006 (2015).
13. E. M. Stewart, J. J. Ague, Pervasive subduction zone devolatilization recycles CO_2 into the forearc. *Nat. Commun.* **11**, 6220 (2020).
14. B. Debret, B. Ménez, B. Walter, H. Bouquerel, P. Bouilhol, N. Mattielli, C. Pisapia, T. Rigaudier, H. M. Williams, High-pressure synthesis and storage of solid organic compounds in active subduction zones. *Sci. Adv.* **8**, eabo2397 (2022).

15. Y. Weiss, C. Class, S. L. Goldstein, T. Hanyu, Key new pieces of the HIMU puzzle from olivines and diamond inclusions. *Nature* **537**, 666–670 (2016).
16. X.-J. Wang, L.-H. Chen, A. W. Hofmann, T. Hanyu, H. Kawabata, Y. Zhong, L.-W. Xie, J.-H. Shi, T. Miyazaki, Y. Hirahara, T. Takahashi, R. Senda, Q. Chang, B. S. Vaglarov, J.-I. Kimura, Recycled ancient ghost carbonate in the Pitcairn mantle plume. *Proc. Natl. Acad. Sci. U.S.A.* **115**, 8682–8687 (2018).
17. H. Beunon, N. Mattielli, L. S. Doucet, B. Moine, B. Debret, Mantle heterogeneity through Zn systematics in oceanic basalts: Evidence for a deep carbon cycling. *Earth Sci. Rev.* **205**, 103174 (2020).
18. X.-Y. Zhang, L.-H. Chen, X.-J. Wang, T. Hanyu, A. W. Hofmann, T. Komiya, K. Nakamura, Y. Kato, G. Zeng, W.-X. Gou, W.-Q. Li, Zinc isotopic evidence for recycled carbonate in the deep mantle. *Nat. Commun.* **13**, 6085 (2022).
19. A. P. Jones, M. Genge, L. Carmody, Carbonate melts and carbonatites. *Rev. Mineral. Geochem.* **75**, 289–322 (2013).
20. G. M. Yaxley, M. Anenburg, S. Tappe, S. Decree, T. Guzmics, Carbonatites: Classification, sources, evolution, and emplacement. *Annu. Rev. Earth Planet Sci.* **50**, 261–293 (2022).
21. S. Tappe, C. D. Beard, A. M. Borst, E. R. Humphreys-Williams, B. F. Walter, G. M. Yaxley, *Kimberlite, Carbonatite and Alkaline Magmatic Systems: Definitions, Origins, and Strategic Mineral Resources in Encyclopedia of Volcanoes* (Elsevier, ed. 3, 2025).
22. S. Tappe, A. Stracke, D. van Acken, H. Strauss, A. Luguet, Origins of kimberlites and carbonatites during continental collision – Insights beyond decoupled Nd-Hf isotopes. *Earth Sci. Rev.* **208**, 103287 (2020).
23. S. R. W. Hulett, A. Simonetti, E. T. Rasbury, N. G. Hemming, Recycling of subducted crustal components into carbonatite melts revealed by boron isotopes. *Nat. Geosci.* **9**, 904–908 (2016).
24. K. Bell, J. Blenkinsop, Nd and Sr isotopic compositions of East African carbonatites: Implications for mantle heterogeneity. *Geology* **15**, 99–102 (1987).
25. C. Chen, Y. Liu, S. F. Foley, M. N. Ducea, D. He, Z. Hu, W. Chen, K. Zong, Paleo-Asian oceanic slab under the North China craton revealed by carbonatites derived from subducted limestones. *Geology* **44**, 1039–1042 (2016).
26. S. Tappe, R. L. Romer, A. Stracke, A. Steenfelt, K. A. Smart, K. Muehlenbachs, T. H. Torsvik, Sources and mobility of carbonate melts beneath cratons, with implications for deep carbon cycling, metasomatism and rift initiation. *Earth Planet. Sci. Lett.* **466**, 152–167 (2017).
27. E. Amsellem, F. Moynier, H. Bertrand, A. Bouyon, J. Mata, S. Tappe, J. M. D. Day, Calcium isotopic evidence for the mantle sources of carbonatites. *Sci. Adv.* **6**, eaba3269 (2020).
28. A. Banerjee, R. Chakrabarti, A. Simonetti, Temporal evolution of $\delta^{44/40}$Ca and $^{87}Sr/^{86}Sr$ of carbonatites: Implications for crustal recycling through time. *Geochim. Cosmochim. Acta* **307**, 168–191 (2021).
29. R. Halama, W. F. McDonough, R. L. Rudnick, K. Bell, Tracking the lithium isotopic evolution of the mantle using carbonatites. *Earth Planet. Sci. Lett.* **265**, 726–742 (2008).
30. S. Braunger, M. A. W. Marks, T. Wenzel, L. Chmyz, R. Guitarrari Azzone, G. Markl, Do carbonatites and alkaline rocks reflect variable redox conditions in their upper mantle source? *Earth Planet. Sci. Lett.* **533**, 116041 (2020).
31. K. A. Evans, The redox budget of subduction zones. *Earth Sci. Rev.* **113**, 11–32 (2012).
32. C. Chen, S. F. Foley, S. Tappe, H. Ren, L. Feng, Y. Liu, Calcium isotopes track volatile components in the mantle sources of alkaline rocks and associated carbonatites. *Earth Planet. Sci. Lett.* **625**, 118489 (2024).
33. E. Amsellem, M. Schiller, M. Klausen, A. Bouyon, V. Rojas, M. Bizzarro, Origin of carbonatites and associated silicate rocks revealed by Mg triple-isotope approach. *Chem. Geol.* **636**, 121663 (2023).
34. Z. Cheng, Z. Zhang, T. Hou, M. Santosh, L. Chen, S. Ke, L. Xu, Decoupling of Mg–C and Sr–Nd–O isotopes traces the role of recycled carbon in magnesiocarbonatites from the Tarim Large Igneous Province. *Geochim. Cosmochim. Acta* **202**, 159–178 (2017).
35. J. Sun, X. K. Zhu, N. S. Belshaw, W. Chen, A. G. Doroshkevich, W. J. Luo, W. L. Song, B. B. Chen, Z. G. Cheng, Z. H. Li, Y. Wang, J. Kynicky, G. M. Henderson, Ca isotope systematics of carbonatites: Insights into carbonatite source and evolution. *Geochem. Perspect. Lett.* **17**, 11–15 (2021).
36. S.-A. Liu, F.-Z. Teng, W. Yang, F.-Y. Wu, High-temperature inter-mineral magnesium isotope fractionation in mantle xenoliths from the North China craton. *Earth Planet. Sci. Lett.* **308**, 131–140 (2011).
37. W. Dai, Z. Wang, Y. Liu, C. Chen, K. Zong, L. Zhou, G. Zhang, M. Li, F. Moynier, Z. Hu, Calcium isotope compositions of mantle pyroxenites. *Geochim. Cosmochim. Acta* **270**, 144–159 (2020).
38. M. A. Antonelli, G. Sartori, A. Giuliani, E. A. Schauble, J. Hoffmann, M. W. Schmidt, Calcium isotope fractionation during melt immiscibility and carbonatite petrogenesis. *Geochem. Perspect. Lett.* **28**, 13–19 (2023).
39. W.-Y. Li, F.-Z. Teng, R. Halama, J. Keller, J. Klaudius, Magnesium isotope fractionation during carbonatite magmatism at Oldoinyo Lengai, Tanzania. *Earth Planet. Sci. Lett.* **444**, 26–33 (2016).
40. K.-F. Qiu, R. L. Romer, Z.-Y. Long, A. E. Williams-Jones, H.-C. Yu, S. Turner, Q.-F. Wang, S.-S. Li, J.-Y. Zhang, H.-R. Duan, J. Deng, The role of an oxidized lithospheric mantle in gold mobilization. *Sci. Adv.* **10**, eado6262 (2024).
41. Y. Hu, F.-Z. Teng, T. Plank, C. Chauvel, Potassium isotopic heterogeneity in subducting oceanic plates. *Sci. Adv.* **6**, eabb2472 (2020).
42. D. P. Santiago Ramos, L. A. Coogan, J. G. Murphy, J. A. Higgins, Low-temperature oceanic crust alteration and the isotopic budgets of potassium and magnesium in seawater. *Earth Planet. Sci. Lett.* **541**, 116290 (2020).
43. K.-C. Xing, F. Wang, F.-Z. Teng, W.-L. Xu, Y.-N. Wang, D.-B. Yang, H.-L. Li, Y.-C. Wang, Potassium isotopic evidence for recycling of surface water into the mantle transition zone. *Nat. Geosci.* **17**, 579–585 (2024).
44. Y. Hu, F.-Z. Teng, C. Chauvel, Potassium isotopic evidence for sedimentary input to the mantle source of Lesser Antilles lavas. *Geochim. Cosmochim. Acta* **295**, 98–111 (2021).
45. K. Wang, D. A. Ionov, Potassium isotope evidence for slab-derived fluids in the sub-arc mantle. *Earth Planet. Sci. Lett.* **619**, 118315 (2023).
46. W. Li, L. A. Coogan, K. Wang, Y. Takahashi, M. Shakouri, Y. Hu, X.-M. Liu, Hydrothermal origin of heavy potassium isotope compositions in altered oceanic crust: Implications for tracing the elemental cycle. *Earth Planet. Sci. Lett.* **625**, 118448 (2024).
47. B. Tuller-Ross, B. Marty, H. Chen, K. A. Kelley, H. Lee, K. Wang, Potassium isotope systematics of oceanic basalts. *Geochim. Cosmochim. Acta* **259**, 144–154 (2019).
48. Y. Hu, F.-Z. Teng, R. T. Helz, C. Chauvel, Potassium isotope fractionation during magmatic differentiation and the composition of the mantle. *J. Geophys. Res. Solid Earth* **126**, e2020JB021543 (2021).
49. B. Tuller-Ross, P. S. Savage, H. Chen, K. Wang, Potassium isotope fractionation during magmatic differentiation of basalt to rhyolite. *Chem. Geol.* **525**, 37–45 (2019).
50. C. A. Parendo, S. B. Jacobsen, J.-I. Kimura, R. N. Taylor, Across-arc variations in K-isotope ratios in lavas of the Izu arc: Evidence for progressive depletion of the slab in K and similarly mobile elements. *Earth Planet. Sci. Lett.* **578**, 117291 (2022).
51. Y. Li, W. Wang, Z. Wu, S. Huang, First-principles investigation of equilibrium K isotope fractionation among K-bearing minerals. *Geochim. Cosmochim. Acta* **264**, 30–42 (2019).
52. H. Zeng, V. F. Rozsa, N. X. Nie, Z. Zhang, T. A. Pham, G. Galli, N. Dauphas, Ab initio calculation of equilibrium isotopic fractionations of potassium and rubidium in minerals and water. *ACS Earth Space Chem.* **3**, 2601–2612 (2019).
53. D. A. Ionov, K. Wang, Potassium distribution and isotope composition in the lithospheric mantle in relation to global Earth's reservoirs. *Geochim. Cosmochim. Acta* **309**, 151–170 (2021).
54. F. Pineau, M. Javoy, C. J. Allegre, Systematic study of isotopes of oxygen, carbon and strontium in carbonatites. *Geochim. Cosmochim. Acta* **37**, 2363–2377 (1973).
55. A. N. Zaitsev, J. Keller, Mineralogical and chemical transformation of Oldoinyo Lengai natrocarbonatites, Tanzania. *Lithos* **91**, 191–207 (2006).
56. J. Madeira, J. Mata, C. Mourão, A. Brum da Silveira, S. Martins, R. Ramalho, D. L. Hoffmann, Volcano-stratigraphic and structural evolution of Brava Island (Cape Verde) based on $^{40}Ar/^{39}Ar$, U–Th and field constraints. *J. Volcanol. Geotherm. Res.* **196**, 219–235 (2010).
57. K. Schweitzer, "Siderophile element systematics and Hf-Os isotope signatures of carbonatites: Insights into the origin of Earth's most unusual magmas," thesis, Durham University, Durham, UK (2019).
58. J. Klaudius, J. Keller, Peralkaline silicate lavas at Oldoinyo Lengai, Tanzania. *Lithos* **91**, 173–190 (2006).
59. K. Bell, J. Keller, *Carbonatite Volcanism: Oldoinyo Lengai and the Petrogenesis of Natrocarbonatites* (Springer Science & Business Media, 2012).
60. E. Ranta, G. Stockmann, T. Wagner, T. Fusswinkel, E. Sturkell, E. Tollefsen, A. Skelton, Fluid–rock reactions in the 1.3 Ga siderite carbonatite of the Grønnedal–Íka alkaline complex, Southwest Greenland. *Contrib. Mineral. Petrol.* **173**, 78 (2018).
61. H. Chen, X.-M. Liu, K. Wang, Potassium isotope fractionation during chemical weathering of basalts. *Earth Planet. Sci. Lett.* **539**, 116192 (2020).
62. W. Li, X.-M. Liu, Y. Hu, F.-Z. Teng, O. A. Chadwick, Potassium isotope fractionation during chemical weathering in humid and arid Hawaiian regoliths. *Geochim. Cosmochim. Acta* **333**, 39–55 (2022).
63. F.-Z. Teng, Y. Hu, J.-L. Ma, G.-J. Wei, R. L. Rudnick, Potassium isotope fractionation during continental weathering and implications for global K isotopic balance. *Geochim. Cosmochim. Acta* **278**, 261–271 (2020).
64. S. Li, W. Li, B. L. Beard, M. E. Raymo, X. Wang, Y. Chen, J. Chen, K isotopes as a tracer for continental weathering and geological K cycling. *Proc. Natl. Acad. Sci. U.S.A.* **116**, 8740–8745 (2019).
65. H. Liu, K. Wang, W.-D. Sun, Y. Xiao, Y.-Y. Xue, B. Tuller-Ross, Extremely light K in subducted low-T altered oceanic crust: Implications for K recycling in subduction zone. *Geochim. Cosmochim. Acta* **277**, 206–223 (2020).
66. K.-F. Qiu, R. L. Romer, Z.-Y. Long, H.-C. Yu, S. Turner, R.-Q. Wan, X.-Q. Li, Z.-Y. Gao, J. Deng, Potassium isotopes as a tracer of hydrothermal alteration in ore systems. *Geochim. Cosmochim. Acta* **368**, 185–196 (2024).

67. T.-Y. Huang, F.-Z. Teng, R. L. Rudnick, X.-Y. Chen, Y. Hu, Y.-S. Liu, F.-Y. Wu, Heterogeneous potassium isotopic composition of the upper continental crust. *Geochim. Cosmochim. Acta* **278**, 122–136 (2020).
68. D. P. Dobson, A. P. Jones, R. Rabe, T. Sekine, K. Kurita, T. Taniguchi, T. Kondo, T. Kato, O. Shimomura, S. Urakawa, In-situ measurement of viscosity and density of carbonate melts at high pressure. *Earth Planet. Sci. Lett.* **143**, 207–215 (1996).
69. K. Bell, G. R. Tilton, Probing the mantle: The story from carbonatites. *Eos, Transact. Am. Geophys. Union* **83**, 273–277 (2002).
70. R. Doucelance, T. Hammouda, M. Moreira, J. C. Martins, Geochemical constraints on depth of origin of oceanic carbonatites: The Cape Verde case. *Geochim. Cosmochim. Acta* **74**, 7261–7282 (2010).
71. M. Berkesi, J. L. Myovela, G. M. Yaxley, T. Guzmics, Carbonatite formation in continental settings via high pressure – high temperature liquid immiscibility. *Geochim. Cosmochim. Acta* **349**, 41–54 (2023).
72. W. E. Jackson, G. E. Brown, C. W. Ponader, X-ray absorption study of the potassium coordination environment in glasses from the $NaAlSi_3O_8$-$KAlSi_3O_8$ binary. *J. Non Cryst. Solids* **93**, 311–322 (1987).
73. B. O. Mysen, The structure of silicate melts. *Annu. Rev. Earth Planet. Sci.* **11**, 75–97 (1983).
74. B.-X. Su, Q.-Q. Pan, Y. Bai, W.-J. Li, M.-M. Cui, K.-N. Pang, Potassium isotope fractionation during silicate-carbonatite melt immiscibility and phlogopite fractional crystallization. *Am. Mineral.* **109**, 591–598 (2024).
75. T. LaTourrette, R. L. Hervig, J. R. Holloway, Trace element partitioning between amphibole, phlogopite, and basanite melt. *Earth Planet. Sci. Lett.* **135**, 13–30 (1995).
76. T. P. Fischer, P. Burnard, B. Marty, D. R. Hilton, E. Füri, F. Palhol, Z. D. Sharp, F. Mangasini, Upper-mantle volatile chemistry at Oldoinyo Lengai volcano and the origin of carbonatites. *Nature* **459**, 77–80 (2009).
77. H. Liu, T. Yang, Y.-Y. Xue, J. Deng, Y. Xiao, H. Sun, F. Tong, K. Wang, Y. Gao, K.-Y. Lin, F. Zhang, X. Jin, W.-D. Sun, Slab dehydration and potassium-lithium recycling in the forearc indicated by potassium and lithium isotope compositions of exhumed metabasites. *Geochim. Cosmochim. Acta* **360**, 16–35 (2023).
78. K. Wang, H. G. Close, B. Tuller-Ross, H. Chen, Global average potassium isotope composition of modern seawater. *ACS Earth Space Chem.* **4**, 1010–1017 (2020).
79. D.-Y. Xiong, X.-L. Wang, W. Li, Y.-F. Zheng, C. R. Anhaeusser, A. Hofmann, D. Wang, J.-Y. Li, Potassium isotope evidence for origin of Archean TTG rocks from seawater-hydrothermally altered oceanic crust. *Geochem. Geophys. Geosyst.* **26**, e2024GC011892 (2025).
80. W. Li, X.-M. Liu, K. Wang, F. J. Fodrie, T. Yoshimura, Y.-F. Hu, Potassium phases and isotopic composition in modern marine biogenic carbonates. *Geochim. Cosmochim. Acta* **304**, 364–380 (2021).
81. D. Zhao, Global tomographic images of mantle plumes and subducting slabs: Insight into deep Earth dynamics. *Phys. Earth Planet. Inter.* **146**, 3–34 (2004).
82. T. Lay, J. Hernlund, B. A. Buffett, Core–mantle boundary heat flow. *Nat. Geosci* **1**, 25–32 (2008).
83. A. P. Nutman, V. C. Bennett, C. R. L. Friend, M. J. Van Kranendonk, A. R. Chivas, Rapid emergence of life shown by discovery of 3,700-million-year-old microbial structures. *Nature* **537**, 535–538 (2016).
84. S. B. Shirey, S. H. Richardson, Start of the Wilson cycle at 3 Ga shown by diamonds from subcontinental mantle. *Science* **333**, 434–436 (2011).
85. A. V. Sobolev, E. V. Asafov, A. A. Gurenko, N. T. Arndt, V. G. Batanova, M. V. Portnyagin, D. Garbe-Schönberg, A. H. Wilson, G. R. Byerly, Deep hydrous mantle reservoir provides evidence for crustal recycling before 3.3 billion years ago. *Nature* **571**, 555–559 (2019).
86. M. A. Antonelli, J. Kendrick, C. Yakymchuk, M. Guitreau, T. Mittal, F. Moynier, Calcium isotope evidence for early Archaean carbonates and subduction of oceanic crust. *Nat. Commun.* **12**, 2534 (2021).
87. A. R. Thomson, M. J. Walter, S. C. Kohn, R. A. Brooker, Slab melting as a barrier to deep carbon subduction. *Nature* **529**, 76–79 (2016).
88. C. J. Hawkesworth, P. A. Cawood, B. Dhuime, T. I. S. Kemp, Earth's continental lithosphere through time. *Annu. Rev. Earth Planet. Sci.* **45**, 169–198 (2017).
89. E. M. Syracuse, P. E. van Keken, G. A. Abers, The global range of subduction zone thermal models. *Phys. Earth Planet. In.* **183**, 73–90 (2010).
90. R. Dasgupta, Ingassing, storage, and outgassing of terrestrial carbon through geologic time. *Rev. Mineral. Geochem.* **75**, 183–229 (2013).
91. C. Chen, M. W. Förster, S. F. Foley, S. S. Shcheka, Carbonate-rich crust subduction drives the deep carbon and chlorine cycles. *Nature* **620**, 576–581 (2023).
92. K. A. Smart, S. Tappe, A. B. Woodland, D. R. Greyling, C. Harris, N. Gussone, Constraints on Archean crust recycling and the origin of mantle redox variability from the $\delta^{44}/^{40}Ca$ - $\delta^{18}O$ - fO_2 signatures of cratonic eclogites. *Earth Planet. Sci. Lett.* **556**, 116720 (2021).
93. R. Bolhar, M. J. Whitehouse, L. Milani, N. Magalhães, S. D. Golding, G. Bybee, L. LeBras, A. Bekker, Atmospheric S and lithospheric Pb in sulphides from the 2.06 Ga Phalaborwa phoscorite-carbonatite complex, South Africa. *Earth Planet. Sci. Lett.* **530**, 115939 (2020).
94. J. Farquhar, H. Bao, M. Thiemens, Atmospheric influence of Earth's earliest sulfur cycle. *Science* **289**, 756–758 (2000).
95. R. A. Cabral, M. G. Jackson, E. F. Rose-Koga, K. T. Koga, M. J. Whitehouse, M. A. Antonelli, J. Farquhar, J. M. D. Day, E. H. Hauri, Anomalous sulphur isotopes in plume lavas reveal deep mantle storage of Archaean crust. *Nature* **496**, 490–493 (2013).
96. H. Delavault, C. Chauvel, E. Thomassot, C. W. Devey, B. Dazas, Sulfur and lead isotopic evidence of relic Archean sediments in the Pitcairn mantle plume. *Proc. Natl. Acad. Sci. U.S.A.* **113**, 12952–12956 (2016).
97. F. Zhang, S. J. Romaniello, T. J. Algeo, K. V. Lau, M. E. Clapham, S. Richoz, A. D. Herrmann, H. Smith, M. Horacek, A. D. Anbar, Multiple episodes of extensive marine anoxia linked to global warming and continental weathering following the latest Permian mass extinction. *Sci. Adv.* **4**, e1602921 (2018).
98. M. M. Joachimski, L. Simon, R. van Geldern, C. Lécuyer, Boron isotope geochemistry of Paleozoic brachiopod calcite: Implications for a secular change in the boron isotope geochemistry of seawater over the Phanerozoic. *Geochim. Cosmochim. Acta* **69**, 4035–4044 (2005).
99. J. M. McArthur, R. J.Howarth, G. A.Shields, Y.Zhou. "Strontium isotope stratigraphy" in *Geologic Time Scale 2020*, F. M.Gradstein, J. G. Ogg, M. D.Schmitz, G. M. Ogg, Eds. (Elsevier, 2020), pp. 211–238.
100. A. E. Moran, V. B. Sisson, W. P. Leeman, Boron depletion during progressive metamorphism: Implications for subduction processes. *Earth Planet. Sci. Lett.* **111**, 331–349 (1992).
101. G. E. Harlow, K in clinopyroxene at high pressure and temperature; an experimental study. *Am. Mineral.* **82**, 259–269 (1997).
102. G. Carnevale, A. Caracausi, A. Correale, L. Italiano, S. G. Rotolo, An overview of the geochemical characteristics of oceanic carbonatites: New insights from Fuerteventura carbonatites (Canary Islands). *Minerals* **11**, 203 (2021).
103. H. Liu, Y.-Y. Xue, J. Geldmacher, K. Hoernle, U. Wiechert, S. An, H.-O. Gu, H. Sun, F. Tian, X. Li, K. Wang, H. Zhu, W.-D. Sun, Potassium isotope evidence for subducted upper and lower oceanic crust in ocean island basalt sources. *Earth Planet. Sci. Lett.* **646**, 119015 (2024).
104. R. Halama, W. F. McDonough, R. L. Rudnick, J. Keller, J. Klaudius, The Li isotopic composition of Oldoinyo Lengai: Nature of the mantle sources and lack of isotopic fractionation during carbonatite petrogenesis. *Earth Planet. Sci. Lett.* **254**, 77–89 (2007).
105. W.-Y. Li, H.-M. Yu, J. Xu, R. Halama, K. Bell, X.-Y. Nan, F. Huang, Barium isotopic composition of the mantle: Constraints from carbonatites. *Geochim. Cosmochim. Acta* **278**, 235–243 (2020).
106. Y.-K. Xu, Y. Hu, X.-Y. Chen, T.-Y. Huang, R. S. Sletten, D. Zhu, F.-Z. Teng, Potassium isotopic compositions of international geological reference materials. *Chem. Geol.* **513**, 101–107 (2019).
107. F. Moynier, Y. Hu, K. Wang, Y. Zhao, Y. Gérard, Z. Deng, J. Moureau, W. Li, J. I. Simon, F.-Z. Teng, Potassium isotopic composition of various samples using a dual-path collision cell-capable multiple-collector inductively coupled plasma mass spectrometer, Nu instruments Sapphire. *Chem. Geol.* **571**, 120144 (2021).
108. Y. Hu, X.-Y. Chen, Y.-K. Xu, F.-Z. Teng, High-precision analysis of potassium isotopes by HR-MC-ICPMS. *Chem. Geol.* **493**, 100–108 (2018).
109. H. Chen, Z. Tian, B. Tuller-Ross, R. L. Korotev, K. Wang, High-precision potassium isotopic analysis by MC-ICP-MS: An inter-laboratory comparison and refined K atomic weight. *J. Anal. At. Spectrom* **34**, 160–171 (2019).
110. R. M. Palin, M. Santosh, W. Cao, S.-S. Li, D. Hernández-Uribe, A. Parsons, Secular change and the onset of plate tectonics on Earth. *Earth Sci. Rev.* **207**, 103172 (2020).
111. B. Dhuime, A. Wuestefeld, C. J. Hawkesworth, Emergence of modern continental crust about 3 billion years ago. *Nat. Geosci.* **8**, 552–555 (2015).
112. C. LaFlamme, J. W. Jamieson, M. L. Fiorentini, N. Thébaud, S. Caruso, V. Selvaraja, Investigating sulfur pathways through the lithosphere by tracing mass independent fractionation of sulfur to the Lady Bountiful orogenic gold deposit, Yilgarn Craton. *Gondwana Res.* **58**, 27–38 (2018).
113. V. J. M. Salters, A. Stracke, Composition of the depleted mantle. *Geochem. Geophys. Geosyst.* **5**, Q05B07 (2004).
114. A. Bouvier, J. D. Vervoort, P. J. Patchett, The Lu–Hf and Sm–Nd isotopic composition of CHUR: Constraints from unequilibrated chondrites and implications for the bulk composition of terrestrial planets. *Earth Planet. Sci. Lett.* **273**, 48–57 (2008).
115. F.-Y. Wu, Y.-H. Yang, Q.-L. Li, R. H. Mitchell, J. B. Dawson, G. Brandl, M. Yuhara, In situ determination of U–Pb ages and Sr–Nd–Hf isotopic constraints on the petrogenesis of the Phalaborwa carbonatite Complex, South Africa. *Lithos* **127**, 309–322 (2011).
116. R. Halama, T. Vennemann, W. Siebel, G. Markl, The Grønnedal-Ika carbonatite–syenite complex, South Greenland: Carbonatite formation by liquid immiscibility. *J. Petrol.* **46**, 191–217 (2005).
117. W. J. Verwoerd, The Goudini carbonatite complex, South Africa: A re-appraisal. *Can. Mineral.* **46**, 825–830 (2008).
118. T. Andersen, Magmatic fluids in the Fen carbonatite complex, S.E. Norway. *Contrib. Mineral. Petrol.* **93**, 491–503 (1986).
119. I. V. Veksler, T. F. D. Nielsen, S. V. Sokolov, Mineralogy of crystallized melt inclusions from Gardiner and Kovdor ultramafic alkaline complexes: Implications for carbonatite genesis. *J. Petrol.* **39**, 2015–2031 (1998).

120. H. Vartiainen, H. Paarma, Geological characteristics of the Sokli carbonatite complex, Finland. *Econ. Geol.* **74**, 1296–1306 (1979).
121. L. Chmyz, R. G. Azzone, E. Ruberti, M. A. W. Marks, T. J. S. dos Santos, Olivines as probes into assimilation of silicate rocks by carbonatite magmas: Unraveling the genesis of reaction rocks from the Jacupiranga alkaline-carbonatite complex, southern Brazil. *Lithos* **416–417**, 106647 (2022).
122. W. P. Nash, Mineralogy and petrology of the Iron Hill carbonatite complex, Colorado. *Geol. Soc. Am. Bull.* **83**, 1361–1382 (1972).
123. L. Ackerman, V. Rapprich, L. Polak, T. Magna, V. T. Mclemore, O. Pour, B. Cejkova, Petrogenesis of silica-rich carbonatites from continental rift settings: A missing link between carbonatites and carbonated silicate melts? *J. Geosci.* **66**, 71–87 (2021).
124. S. Braunger, M. A. W. Marks, B. F. Walter, R. Neubauer, R. Reich, T. Wenzel, A. Parsapoor, G. Markl, The petrology of the Kaiserstuhl volcanic complex, SW Germany: The importance of metasomatized and oxidized lithospheric mantle for carbonatite generation. *J. Petrol.* **59**, 1731–1762 (2018).
125. K. Hoernle, G. Tilton, M. J. Le Bas, S. Duggen, D. Garbe-Schönberg, Geochemistry of oceanic carbonatites compared with continental carbonatites: Mantle recycling of oceanic crustal carbonate. *Contrib. Mineral. Petrol.* **142**, 520–542 (2002).
126. T. Guzmics, Z. Zajacz, R. H. Mitchell, C. Szabó, M. Wälle, The role of liquid–liquid immiscibility and crystal fractionation in the genesis of carbonatite magmas: Insights from Kerimasi melt inclusions. *Contrib. Mineral. Petrol.* **169**, 17 (2015).
127. Z.-Y. Ding, S.-K. Liu, B.-X. Su, W.-J. Li, Y. Bai, Q.-Q. Pan, F.-Y. Hu, K.-N. Pang, Potassium isotope fractionation during granite differentiation and implications for crustal K isotope heterogeneity. *Lithos* **448-449**, 107176 (2023).
128. T.-Y. Huang, F.-Z. Teng, Z.-Z. Wang, Y.-S. He, Z.-C. Liu, F.-Y. Wu, Potassium isotope fractionation during granitic magmatic differentiation: Mineral-pair perspectives. *Geochim. Cosmochim. Acta* **343**, 196–211 (2023).
129. Z.-Z. Wang, F.-Z. Teng, F.-Y. Wu, Z.-C. Liu, X.-C. Liu, S.-A. Liu, T.-Y. Huang, Extensive crystal fractionation of high-silica magmas revealed by K isotopes. *Sci. Adv.* **8**, eabo4492 (2022).
130. H. Xu, W. Li, X.-L. Wang, J. Mu, D.-H. Du, J.-L. Zhao, D.-Y. Xiong, Tracing magmatic differentiation of peralkaline granites by using K stable isotopes. *Geochim. Cosmochim. Acta* **366**, 154–166 (2024).
131. W. Li, S. Li, B. L. Beard, Geological cycling of potassium and the K isotopic response: Insights from loess and shales. *Acta Geochim.* **38**, 508–516 (2019).
132. H. Liu, Y.-Y. Xue, G. Zhang, W.-D. Sun, Z. Tian, B. Tuller-Ross, K. Wang, Potassium isotopic composition of low-temperature altered oceanic crust and its impact on the global K cycle. *Geochim. Cosmochim. Acta* **311**, 59–73 (2021).
133. Y.-D. Liu, Z. Guo, H.-C. Tian, G. Qin, X. Peng, Potassium isotopic fractionation during multistage alteration of oceanic crust in the southern Mariana Trench. *Chem. Geol.* **620**, 121350 (2023).
134. C. A. Parendo, S. B. Jacobsen, K. Wang, K isotopes as a tracer of seafloor hydrothermal alteration. *Proc. Natl. Acad. Sci. U.S.A.* **114**, 1827–1831 (2017).
135. H.-C. Tian, F.-Z. Teng, X.-Y. Chen, Z.-X. Guo, X.-T. Peng, W. Yang, Y.-L. Xiao, Multi-mode chemical exchange in seafloor alteration revealed by lithium and potassium isotopes. *Chem. Geol.* **606**, 121004 (2022).
136. C. A. Parendo, S. B. Jacobsen, T. Plank, Potassium-isotope variations of marine sediments adjacent to the Izu-Bonin Trench and Nankai Trough. *Geochim. Cosmochim. Acta* **337**, 166–181 (2022).
137. W. Li, X.-M. Liu, K. Wang, J. McManus, B. A. Haley, Y. Takahashi, M. Shakouri, Y. Hu, Potassium isotope signatures in modern marine sediments: Insights into early diagenesis. *Earth Planet. Sci. Lett.* **599**, 117849 (2022).
138. L. E. Morgan, D. P. S. Ramos, B. Davidheiser-Kroll, J. Faithfull, N. S. Lloyd, R. M. Ellam, J. A. Higgins, High-precision 41K/39K measurements by MC-ICP-MS indicate terrestrial variability of δ41K. *J. Anal. At. Spectrom* **33**, 175–186 (2018).
139. W. Li, X.-M. Liu, K. Wang, Y. Hu, A. Suzuki, T. Yoshimura, Potassium incorporation and isotope fractionation in cultured scleractinian corals. *Earth Planet. Sci. Lett.* **581**, 117393 (2022).
140. R. L. Cullers, Implications of elemental concentrations for provenance, redox conditions, and metamorphic studies of shales and limestones near Pueblo, CO, USA. *Chem. Geol.* **191**, 305–327 (2002).
141. H. Palme, H. St. C. O'Neill, "Cosmochemical Estimates of Mantle Composition" in *Treatise on Geochemistry*, H. D. Holland, K. K. Turekian, Eds. (Pergamon, 2007), pp. 1–38.
142. K. A. Kelley, T. Plank, J. Ludden, H. Staudigel, Composition of altered oceanic crust at ODP Sites 801 and 1149. *Geochem. Geophys. Geosyst.* **4**, 8910 (2003).
143. X.-K. Wang, X.-M. Liu, H. Chen, An efficient method for high-precision potassium isotope analysis in carbonate materials. *J. Anal. At. Spectrom* **37**, 2410–2419 (2022).

Acknowledgments: We thank T.-H. Luu and D. Rigoussen for assistance with the experiments. This work was partly supported by the IPGP analytical platform PARI, Region Ile-de-France SESAME grant no. 12015908 and the DIM ACAV +. We are also indebted to Y. Hu for insightful discussions during the early stages of this study. **Funding:** This work was supported by the National Key Research and Development Program of China (2023YFF0804200 to K.-F.Q.), the European Research Council [no. 101001282 (METAL) to F.M.], and the China Scholarship Council (202206400044 to Z.-Y.L.). **Author contributions:** Conceptualization: Z.-Y.L., F.M., and S.T. Methodology: Z.-Y.L., F.M., B.D., and H.-X.S. Formal analysis: Z.-Y.L. and W.D. Data curation: Z.-Y.L. Investigation: Z.-Y.L. and B.D. Visualization: Z.-Y.L. Supervision: F.M. Resources: F.M., H.B., K.B., E.I., and S.T. Funding acquisition: K.-F.Q., F.M., and Z.-Y.L. Validation: Z.-Y.L., F.M., and K.-F.Q. Project administration: F.M. Writing—original draft: Z.-Y.L. and B.D. Writing—review and editing: Z.-Y.L., F.M., B.D., K.-F.Q., W.D., H.-X.S., J.D., H.B., K.B., E.I., and S.T. **Competing interests:** The authors declare that they have no competing interests. **Data and materials availability:** All data needed to evaluate the conclusions in the paper are present in the paper and/or the Supplementary Materials.

Submitted 11 September 2024
Accepted 9 May 2025
Published 13 June 2025
10.1126/sciadv.adt1023